Published November 8, 2010

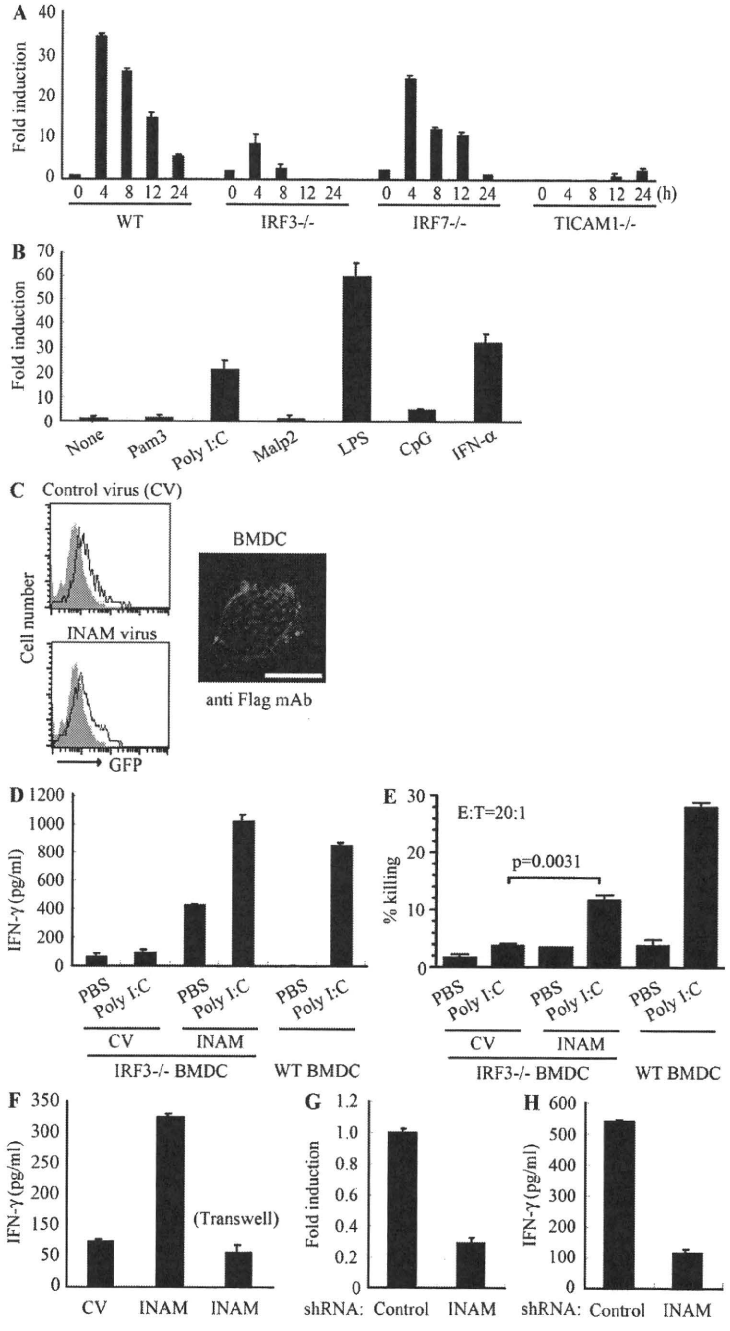

Figure 3. INAM in BMDC participates in DC-mediated NK activation. (A) Quantitative RT-PCR for INAM expression in WT, TICAM-1$^{-/-}$, IRF-3$^{-/-}$, and IRF-7$^{-/-}$ BMDC stimulated with 10 µg/ml polyI:C. (B) Quantitative RT-PCR for INAM expression in WT BMDC stimulated by 100 ng/ml LPS, 10 µg/ml polyI:C, 1 µg/ml Pam3, 100 nM Malp-2, 10 µg/ml CpG, and 2,000 IU/ml IFN-α for 4 h. (C) BMDCs were transduced with Flag-tagged INAM-expressing lentivirus or control lentivirus. GFP expression in the BMDC was determined by flow cytometry, and subcellular localization of INAM was examined by immunofluorescence assay using anti-Flag mAb. Shaded peak, noninfected control; Blank peak, infected BMDC. Bar, 10 µm. (D) ELISA of IFN-γ induced by WT NK cells co-cultured with WT BMDC or IRF-3$^{-/-}$ BMDC transfected with control lentivirus (CV) or INAM-expressing lentivirus (INAM) with/without 10 µg/ml polyI:C. (E) Cytotoxicity against B16D8 by NK cells co-cultured with BMDC transfected with control or INAM-expressing lentivirus with/without 10 µg/ml polyI:C for 24 h. (F) ELISA of IFN-γ induced by WT NK cells co-cultured with IRF-3$^{-/-}$ BMDC transfected with control lentivirus (CV) or INAM-expressing lentivirus (INAM) with 10 µg/ml polyI:C. In some experiments, a transwell was inserted between the INAM-transduced BMDC and NK cells to separate the cells. (G) Quantitative RT-PCR for expression of INAM in BMDC transduced with INAM-shRNA (INAM) or scrambled shRNA (control) and cultured for 48 h. (H) IFN-γ production by WT NK cells determined using ELISA after coculturing with control or the shRNA transfected-BMDC (INAM) and 10 µg/ml polyI:C for 24 h. All data shown are means ± SD of triplicate samples from one experiment that is representative of three.

detected by ELISA (unpublished data). In addition, polyI:C-mediated NK activation occurred in BMDC expressing an INAM mutant lacking the cytoplasmic C-terminal region (193–327 aa; Fig. 4, A and B), excluding the participation of the cytoplasmic region in BMDC maturation signaling.

To investigate whether INAM could reconstitute NK-activating ability in IRF-3$^{-/-}$ BMDC, we transduced INAM into IRF-3$^{-/-}$ BMDC and incubated BMDC with NK cells. Overexpression of INAM in IRF-3$^{-/-}$ BMDC induced NK IFN-γ production and NK cytotoxicity against B16D8, and this NK activation was further enhanced by the addition of polyI:C (Fig. 3, D and E). Thus, polyI:C may also work for NK activation. Direct cell–cell contact with NK cells was required for INAM in IRF-3$^{-/-}$ BMDC to function on enhancing NK activity (Fig. 3 F).

We further confirmed this issue using WT BMDC by shRNA gene silencing. We silenced the INAM gene in BMDC using the lentiviral vector pLenti-dest-IRES-hrGFP and monitored expression by GFP. Because transfection efficiency was relatively high in this case compared with that shown in Fig. 3 C, the expression level of INAM had decreased by ~75% in WT BMDC compared with the nonsilenced control (Fig. 3 G and Fig. S6 A). Although the level of the endogenous INAM protein was not very high, we confirmed that INAM protein was also decreased by shRNA with immunoblotting using anti-INAM pAb (Fig. S7 A). PolyI:C response of BMDC-inducible cytokines tested was not altered by INAM silencing in BMDC (Fig. S6 B). Yet this INAM RNA interference caused a significant decrease in NK cell IFN-γ production after co-culture of the INAM knockdown BMDCs and WT NK cells with polyI:C (Fig. 3 H). Collectively, these results indicate that INAM is downstream of IRF-3 in BMDC and is involved in the activation of NK cells by BMDC.

Published November 8, 2010

Using an INAM-expressing stable BaF3 cell line (INAM/BaF3), we tested the possibility that INAM is an activating ligand for NK cells. As a positive control, we produced a stable BaF3 cell line expressing Rae-1α (Fig. 5 A) which is a ligand for the NK-activating receptor NKG2D (Cerwenka et al., 2000). Although Rae-1α/BaF3 cells were easily damaged by IL-2–activated NK cells, INAM/BaF3 cells were not (Fig. 5 B). In this context, addition of IRF-3$^{-/-}$ BMDC to this culture with BaF3 and NK cells led to slight augmentation of IFN-γ induction irrespective of the presence of INAM on BaF3 cells (Fig. 5 C), and β2-microglobulin$^{-/-}$ BMDC barely affected the IFN-γ level (not depicted). These results suggest that an INAM-containing molecular matrix, rather than INAM alone, acts toward NK cells. Alternatively, INAM may selectively function with specific mDC molecules to activate NK cells.

INAM on NK cells is required for efficient NK activation

mDCs were previously shown to be required for efficient NK activation in vivo and in vitro (Akazawa et al., 2007a). We found that INAM was minimally present in BMDCs and NK cells and that polyI:C acts on both (Figs. S2 A; and Fig 3, D and E). Tetraspanin-like molecules tend to work as scaffolds for heteromolecular complexes that contain molecules functioning in a cis- or trans-adhesion manner to exert intercellular or extracellular functions. Thus, the function of INAM may not be confined to mDC, so we studied the function of INAM on NK cells. In NK cells, INAM was also inducible by polyI:C (Fig. 6 A and Fig. S2 A), and the induction of INAM was abrogated completely in IRF-3$^{-/-}$ NK cells and moderately in TICAM1$^{-/-}$ NK cells (Fig. 6 B). This suggests that polyI:C also acts on NK cells and induces INAM through IPS-1/IRF-3 activation when NK cells are co-cultured with BMDC and polyI:C.

To investigate whether INAM induced in NK cells is associated with BMDC-mediated NK activation, we performed the following experiments (Fig. 6 C). INAM-transduced IRF-3$^{-/-}$ BMDCs were incubated with polyI:C for 4 h, and then the aliquot was mixed with WT NK cells in the presence of polyI:C (Fig. 6 C, left two lanes). A moderate increase of IFN-γ was observed as in Fig. 3 D. In the remainder,

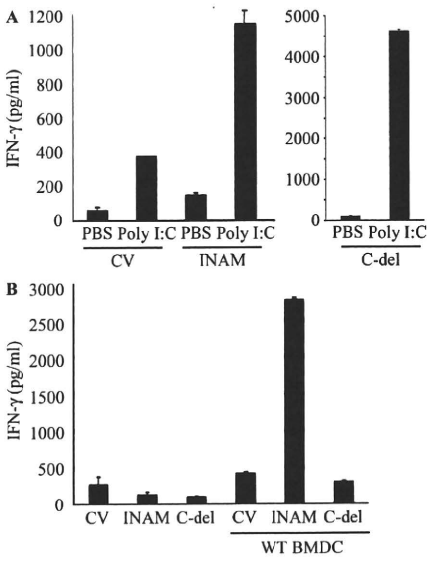

Figure 4. Role of the cytoplasmic tail of INAM. (A) The C-terminal region of INAM was not required for BMDC-mediated NK activation. ELISA of IFN-γ by WT NK cells co-cultured with IRF-3$^{-/-}$ BMDCs transfected with control lentivirus (CV) or a lentivirus expressing intact INAM or a mutant INAM lacking the C-terminus (C-del INAM) with/without 10 μg/ml polyI:C. Data shown are means ± SD of triplicate samples from one experiment representative of three. (B) The cytoplasmic tail of INAM is indispensable for NK IFN-γ induction. INAM or C-del INAM (A) was expressed on IRF-3$^{-/-}$ NK cells. The INAM (or C-del INAM)-expressing IRF-3$^{-/-}$ NK cells were incubated with or without WT BMDC for 24 h. IFN-γ levels in the supernatants were determined by ELISA. One representative result out of several similar experiments is shown. Data represent mean ± SD.

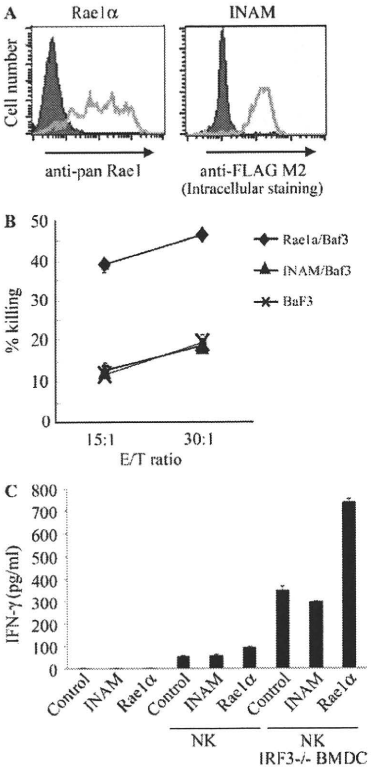

Figure 5. INAM is not an NK-activating ligand. (A) Flow cytometry for Rae-1 and Flag-tagged INAM in stable BaF3 lines. Shaded peak, untransfected control BaF3 staining with anti-pan-Rae-1 Ab or anti-Flag M2 antibody; open peak, stable Rae-1α/BaF3 or stable Flag-tagged INAM/BaF3 staining with anti-pan-Rae-1 antibody or anti-Flag M2 antibody. (B) Cytotoxicity against control BaF3, Rae-1α/BaF3, and INAM/BaF3 by NK cells treated with 1,000 IU/ml IL-2 for 3 d. Data shown are means ± SD of triplicate samples from one experiment representative of three. (C) NK activation is augmented by coexistent BMDC irrespective of INAM expression. NK cells were cultured with 1,000 IU/ml IL-2 for 3 d. 2 × 10^5 NK cells, 10^5 BaF3 cells, and 10^5 IRF-3$^{-/-}$ BMDCs were co-cultured in 200 μl/well and IFN-γ in the supernatants were measured by ELISA. Data show one of two similar experimental results. Data represent mean ± SD.

Published November 8, 2010

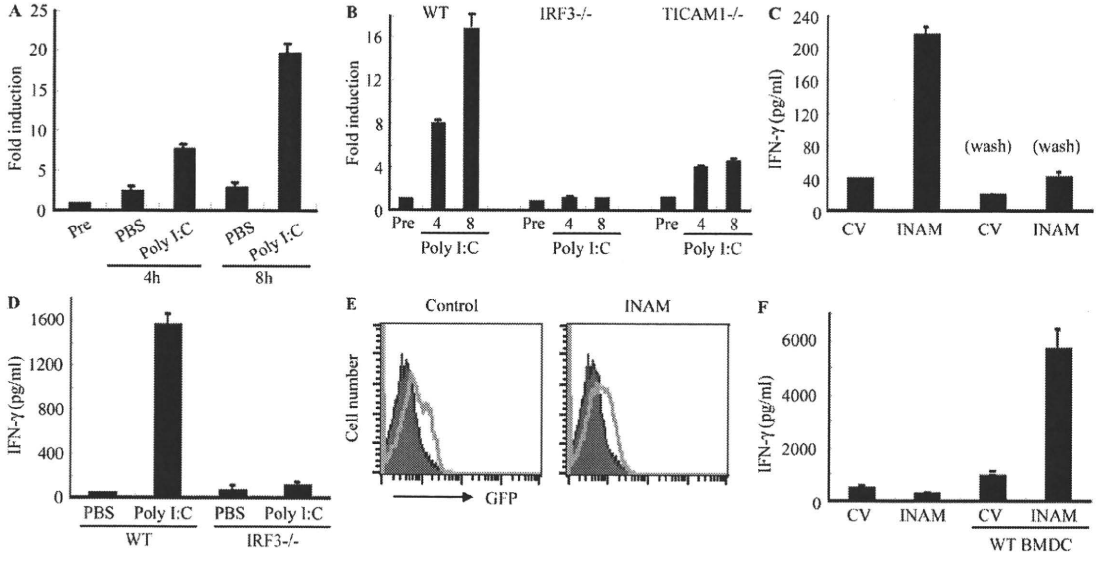

Figure 6. INAM on NK cells contributes to efficient NK activation mediated by mDC. (A and B) Quantitative RT-PCR for INAM expression in WT, TICAM1$^{-/-}$, or IRF-3$^{-/-}$ NK cells stimulated with 50 µg/ml polyI:C. Data shown are means of duplicate or triplicate samples from one experiment that is representative of three. (C) IRF-3$^{-/-}$ BMDCs were transfected with control lentivirus (CV) or INAM-expressing lentivirus (INAM) before treatment with 10 µg/ml polyI:C for 4 h. BMDCs in some wells were washed to remove polyI:C before WT NK cells were added (Wash). IFN-γ production by NK cells was determined by ELISA after 24 h of culture. Data show one of two similar experimental results. (D) ELISA of IFN-γ in co-culture of WT or IRF-3$^{-/-}$ NK cells and WT BMDC with/without 10 µg/ml polyI:C. (E and F) NK cells were transfected with control lentivirus or INAM-expressing lentivirus and cultured with 500 IU/ml IL-2 for 3 d. After determining transfection efficiency by GFP intensity using flow cytometry, cells were cultured with/without BMDC for 24 h and IFN-γ production in the supernatant determined by ELISA. Shaded peak, noninfected control; open peak, infected BMDC. All data are means ± SD of triplicate samples from one experiment that is representative of three.

we washed polyI:C out and cultured the cells with WT NK cells (Fig. 6 C, right two lanes). Under these conditions, in which polyI:C acted not on NK cells but only on BMDC, little NK activation was observed (Fig. 6 C). Furthermore, IRF-3$^{-/-}$ NK cells produced little IFN-γ when co-cultured with WT BMDC and polyI:C (Fig. 6 D). INAM-overexpressing IRF-3$^{-/-}$ BMDC required IRF-3 in NK cells for efficient BMDC-mediated production of IFN-γ from NK cells (Fig. 6 D). We next transduced INAM into IRF-3$^{-/-}$ NK cells using a lentivirus (INAM/pLenti-IRES-hrGFP) to reconstitute NK IFN-γ–producing activity. After many trials with various setting conditions, we found that ~15% of the DX5^{+} NK cell population was both GFP-positive and stained with anti-FLAG mAb when treated with high doses of INAM-expressing lentivirus vector (Fig. S7 B). When IRF-3$^{-/-}$ NK cells were infected with smaller amounts of INAM-expressing lentiviral vector and cultured for 3 d with high concentrations of IL-2 (500 IU/ml), slight but significant GFP expression was confirmed by FACS (Fig. 6 E). Then, the INAM-transduced IRF-3$^{-/-}$ NK cells were co-cultured with WT BMDC. The IRF-3$^{-/-}$ NK cells with INAM expression secreted IFN-γ at significantly higher levels than controls in the presence of WT BMDC (Fig. 6 F). These data indicate that INAM is induced by polyI:C through IRF-3 activation, not only in BMDCs but also in NK cells, and that INAM on NK cells synergistically works with INAM on BMDC for efficient NK cell activation. Both INAMs on BMDC and NK cells are essential for BMDC-mediated NK activation.

We next checked the function of the C-terminal stretch of INAM in NK activation. Although intact INAM works in NK cells to produce IFN-γ in response to BMDC (Fig. 6 F), introduction of C-del INAM into IRF-3$^{-/-}$ NK cells did not result in high induction of IFN-γ in response to BMDC (Fig. 4 C). Thus, INAM participates in NK activation through its cytoplasmic regions, which has no significant role in BMDC for NK activation.

Anti-tumor NK activation via INAM-expressing BMDCs in vivo

mDC-mediated NK activation induces anti-tumor NK cells, which cause regression of NK-sensitive tumors (Kalinski et al., 2005; Akazawa et al., 2007a). We tested the in vivo function of INAM-expressing BMDC using B16D8 tumor-bearing mice. BMDCs were used 24 h after transfection with either INAM/pLenti-IRES-hrGFP or control pLenti-IRES-hrGFP and injected twice a week s.c. around a preexisting tumor in tumor-implanted mice, beginning 11–13 d after tumor challenge. INAM-expressing BMDC significantly retarded tumor growth (Fig. 7 A). Tumor retardation was abrogated by depletion of NK1.1-positive cells (Fig. 7 B). Thus, INAM expression on BMDC contributed to anti-tumor NK activation in vivo.

When the control or INAM-expressing IRF-3$^{-/-}$ BMDCs were co-cultured with WT NK cells in vitro, there was no induction of the mRNA of TRAIL and granzyme B in

Published November 8, 2010

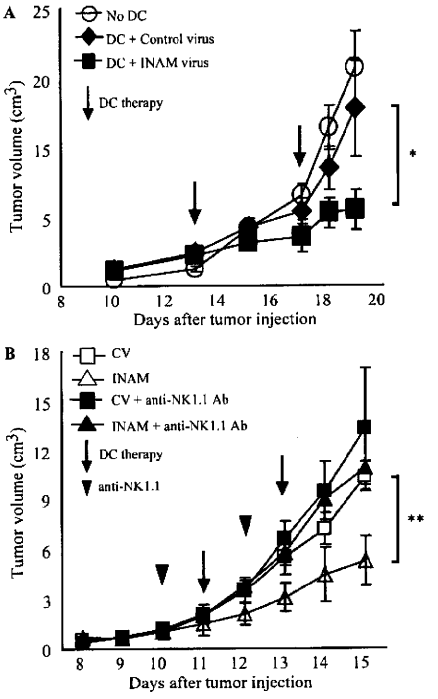

Figure 7. INAM on BMDC retarded B16D8 tumor growth in an NK-dependent manner. (A) Tumor volume after DC therapy using BMDC expressing INAM. B16D8 cells were s.c. injected into C57BL/6 mice and, 11–13 d later, medium only (○) or BMDC (10^6/mouse) transfected with control lentivirus (◆) or those with INAM-expressing lentivirus (■) were administered s.c. near the tumor at the time indicated by the open arrow. *, P = 0.043. Data represent mean ± SD. (B) Abrogation of INAM-dependent tumor regression by administration of NK1.1 Ab. For depletion of NK cells, antiNK1.1 mAb was injected i.p. 1 d before treatment of BMDC (arrowheads). Tumor volume in every mouse group was sequentially monitored. Data represent mean ± SD (n = 3) and are representative of two experiments. Statistical analyses were made with the Student's t test. **, P = 0.017.

NK cells (Fig. 8 A). TRAIL and granzyme B were induced in NK cells by the addition of polyI:C to the mixture, and INAM expression in BMDC up-regulated mRNA levels of TRAIL and granzyme B (Fig. 8 A). In vivo administration studies were performed with polyI:C-treated WT BMDC or INAM-expressing IRF-$3^{-/-}$ BMDC to test their ability to up-regulate the mRNA levels of TRAIL and granzyme B in NK cells in draining LN (Fig. 8 B). INAM-expressing IRF-$3^{-/-}$ BMDC showed comparable abilities to up-regulate the killing effectors with polyI:C-treated BMDC (Fig. 8 B). Collectively, INAM has therapeutic potential for NK-sensitive tumors by activating NK cells.

DISCUSSION

Previous studies demonstrated that mDC–NK interaction leads to direct NK activation and damages NK target cells in vitro (Gerosa et al., 2002; Sivori et al., 2004; Akazawa et al., 2007a; Lucas et al., 2007). In addition, mDCs initiate NK cell–mediated innate anti-tumor immune responses in vivo (Kalinski et al., 2005; Akazawa et al., 2007a,b). Systemic administration of polyI:C unequivocally results in activation of peripheral NK cells (Lee et al., 1990; Sivori et al., 2004; Akazawa et al., 2007a). Although the molecular mechanism by which mDCs prime NK cells was still unclear, the TICAM-1 pathway and IPS-1 pathway have been reported to participate in polyI:C-mediated mDC maturation that drives NK activation (Akazawa et al., 2007a; McCartney et al., 2009; Miyake et al., 2009). We have shown in an earlier study that mDCs disrupted in the TLR3–TICAM-1 pathway abrogate NK cell activation (Akazawa et al., 2007a,b). In TICAM-$1^{-/-}$ mice, NK-sensitive implant tumors grew as well as those in WT mice depleted of NK cells (Akazawa et al., 2007a). mDCs gain high anti-tumor potential against B16D8 implant tumors through lentiviral transfer of TICAM-1, which is attributable to NK activation (Akazawa et al., 2007a). We further showed that TICAM-1 is a critical molecule for mDC to induce NK cell IFN-γ, as well as IPS-1, and participates in driving NK cytotoxicity to a lesser extent than IPS-1. In this paper, we clarified a molecular mechanism by which mDCs immediately promote NK cell functions in vitro and in vivo.

Our findings showed that IRF-3 is the transcription factor that is downstream of TICAM-1 responsible for maturing mDC to an NK-activating phenotype. We discovered that INAM, a membrane-associated protein, is up-regulated on the surface of mDC by polyI:C stimulation and activates NK cells via cell–cell contact. Furthermore, we found that NK cells also express INAM on their cell surface after polyI:C stimulation. mDC–NK activation by polyI:C can be reproduced with INAM-transduced mDC and NK cells, and adoptive transfer experiments show that INAM-overexpressing mDC may have therapeutic potential against MHC-low melanoma cells in an NK-dependent manner. These functional properties of INAM-expressing mDC fit the model of mDC priming NK activation. Ultimately, INAM appears to be the key molecule in the previously reported mechanism of mDC–NK contact activation.

After the submission of this manuscript, two papers were published that found that the MDA5–IPS-1 pathway in mDC is more important for driving NK activation, particularly in vivo (McCartney et al., 2009; Miyake et al., 2009). Our data also support this point using the IPS-$1^{-/-}$ mice we established (Fig. S1). However, polyI:C, when i.v. administered into mice, may stimulate other systemic cells in addition to $CD8^+$ mDC in vivo (McCartney et al., 2009). The difference among the two (McCartney et al., 2009; Miyake et al., 2009) and this study may be attributed to the setting conditions, which are not always comparable. Moreover, it remains to be settled whether TICAM-1 and IPS-1 take the same INAM complex as a common NK activator in mature mDC and whether TLR3 (or MDA5) KO is equivalent to TICAM-1 (or IPS-1) KO in the mDC–NK activation model. In either case, however, up-regulation of mDC TICAM-1–mediated NK cytotoxicity and IFN-γ induction are feasible with polyI:C under three different conditions (Akazawa et al., 2007a; McCartney et al., 2009; Miyake et al., 2009). Our results infer that INAM participates in at least these mDC–NK interactions.

Published November 8, 2010

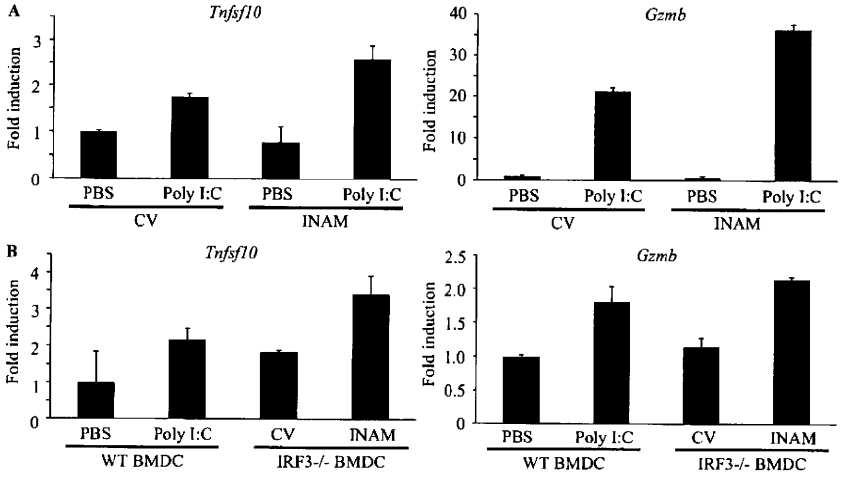

Figure 8. INAM-mediated induction of TRAIL and granzyme B in BMDC. (A) In vitro induction of TRAIL (Tnfsf10) and granzyme B (Gzmb) mRNA by INAM-expressing BMDC. BMDCs (IRF-3$^{-/-}$) were infected with INAM-expressing virus or CV as in Fig. S4. After 24 h, the BMDCs (IRF-3$^{-/-}$) were incubated with WT NK cells at DC/NK = 1:2. 8 h later, DX5$^+$ cells were collected by FACS sorting and their RNA was extracted to determine the mRNA levels of the indicated genes. A representative result of three similar experiments are shown. (B) In vivo induction of TRAIL and granzyme B mRNA by INAM-expressing BMDC. WT BMDCs were stimulated with 10 μg/ml polyI:C or medium only. IRF-3$^{-/-}$ BMDCs were infected with CV or INAM-expressing vector. These BMDCs were allowed to stand for 24 h and then 5 × 10^5 cells were injected into footpads of WT mice. After 48 h, DX5$^+$ cells were collected from the inguinal LN by FACS sorting. RNA of the cells was extracted and the levels of the indicated mRNA were determined by real time PCR. Data show one of two experiments with similar results. Data in A and B represent mean ± SD.

PolyI:C activates IRF-3 through the two pathways involving the adaptors IPS-1 and TICAM-1 (Yoneyama et al., 2004; Kato et al., 2006; Matsumoto and Seya, 2008). The two pathways share the complex of IRF-3–activating kinase, NAP1, IKK-ε, and TBK1 that is downstream of adaptors (Sasai et al., 2006). Nevertheless, these pathways are capable of inducing several genes unique to each adaptor. Although IFN-α production by in vivo administration of polyI:C is largely dependent on the IPS-1 pathway, IL-12p40 is mainly produced by the TICAM-1 pathway (Kato et al., 2006). Therefore, it is not surprising that INAM induction is predominant in the TICAM-1 pathway in polyI:C-stimulated BMDC (Fig. 3 A). What happens in IRF-7$^{-/-}$ BMDCs in terms of INAM induction and what mechanism sustains BMDC IPS-1–mediated or MyD88-mediated activation of NK cells (Azuma et al., 2010) will be issues to be elucidated in the future.

Although IRF-3–regulated cell surface INAMs are required for efficient interaction between BMDC and NK cells, the mechanism by which forced expression of INAM causes signaling for BMDC maturation is still unknown. Although the NK-activating capacity of BMDCs is usually linked to their maturation, neither cytokines in NK activation, including IFN-α and IL-12p70, nor costimulators, such as CD40 and CD86, were specifically induced in mDC by INAM expression (Fig. S5). INAM has a C-terminal cytoplasmic stretch (Fig. 4 A), and we tested the function of this region by a deletion mutant (C-del INAM). This region in BMDC barely participates in driving NK activation because no decrease of IFN-γ induction by NK cells was observed with IRF-3$^{-/-}$ BMDC supplemented with C-del INAM compared with control INAM. Thus far, no significant signal alteration has been detected in BMDC supplemented with INAM by lentivirus.

In contrast, INAM-transduced IRF-3$^{-/-}$ NK cells produced IFN-γ in concert with BMDCs like WT NK cells (Fig. 6 F). So far we have no evidence suggesting that this kind of INAM overexpression is actually occurring in vivo. However, introduction of C-del INAM into IRF-3$^{-/-}$ NK cells did not result in high induction of IFN-γ in response to BMDC (Fig. 4 C). Together with the data on INAM expression in BMDC, this infers that the INAM cytoplasmic region signals for NK activation in NK cells. The one-way role of the cytoplasmic tail in NK activation will be an issue for further analysis.

In this study, IL-15 was found to be up-regulated by polyI:C in BMDC. The remaining NK activity in the resting population of NK cells co-cultured with TICAM-1$^{-/-}$ BMDC and polyI:C (Fig. 1 B) suggests that IL-15 has some effect in our system, and other studies suggest this as well (Ohteki et al., 2006; Brilot et al., 2007; Lucas et al., 2007; Huntington et al., 2009). However, we did not observe decreased IL-15 expression in the TICAM-1$^{-/-}$ BMDC that could not activate NK cells (Fig. 1 E). Several molecules, such as B7-H6/NKp30 (Brandt et al., 2009), CD48/2B4 (Kubin et al., 1999), and NKG2D ligands/NKG2D (Cerwenka et al., 2000), have been identified as ligand/receptor molecules in mDC–NK reciprocal activation by in vitro co-culture. In in vitro co-culture systems (Fig. S1), the IPS-1 pathway in BMDC has a pivotal role in not only type I IFN but also IL-15 induction. INAM identified in this paper serves a unique function in the in vivo induction of NK activation and may offer a tool to investigate the reported mDC-mediated NK activation.

Rae-1 was reported as a molecule with MHC-like structure (Zou et al., 1996) and later identified as a mouse NKG2D ligand (Cerwenka et al., 2000). Although Rae-1 is a GPI-anchored protein with no cytoplasmic sequences (Nomura et al., 1996), it can act as an NK-activating ligand (Cerwenka et al., 2000, 2001; Masuda et al., 2002). Mouse BaF3 cells become NK-sensitive after forced expression of Rae-1α (Masuda et al., 2002). Actually, mouse macrophages induce Rae-1 expression in response to TLR stimuli (Hamerman et al., 2004). In contrast,

Published November 8, 2010

INAM-expressing stable BaF3 cell lines (INAM/BaF3) did not reveal a function as an NK cell–activating ligand. NK cell cytotoxicity is directed against Rae-1α/BaF3 cells but not against INAM/BaF3 cells (Fig. 5). Therefore, INAM does not represent a typical NK cell–activating ligand. For NK activation, INAM on BMDC appears to require other molecules that are expressed in BMDC but not in BaF3.

INAM has four transmembrane regions, similar to the cell adhesion tetraspanins, which may support cell–cell contact (Levy and Shoham, 2005). Tetraspanins provide a scaffold that facilitates complex formation with associated proteins. INAM on BMDC and NK cells may use cell–cell interaction to assemble in a synaptic formation to activate NK cells. Because the protein constituents of the tetraspanin complexes are cell specific, we are interested in finding partners for INAM that might participate in efficient BMDC–NK interaction. TLR-inducible cell–cell contact may occur through INAM in an immune cell–specific manner. Gene disruption of this INAM will facilitate clarifying this issue. The identification of INAM defines a novel pathway in mDC–NK reciprocal interaction. This study will lead to further research on the molecules that form complexes on BMDC and NK cells to facilitate BMDC–NK interaction.

MATERIALS AND METHODS

Mice. All mice were backcrossed with C57BL/6 mice more then seven times before use. TICAM-1$^{-/-}$ (Akazawa et al., 2007a) and IPS-1$^{-/-}$ mice were generated in our laboratory. IRF-3$^{-/-}$ (Sato et al., 2000) and IRF-7$^{-/-}$ mice (Honda et al., 2005) were provided by T. Taniguchi (University of Tokyo, Tokyo, Japan). All mice were maintained under specific pathogen-free conditions in the animal facility of the Hokkaido University Graduate School of Medicine. Animal experiments protocols and guidelines were approved by the Animal Safety Center, Hokkaido University, Japan.

Cells. The B16D8 cell line was established in our laboratory as a subline of B16 melanoma (Tanaka et al., 1988). This subline was characterized by its low or virtually no metastatic properties when injected s.c. into syngeneic C57BL/6 mice. B16D8 was cultured in RPMI 1640/10% FCS. The mouse B cell line BaF3 was obtained from American Type Culture Collection and cultured in RPMI 1640/10% FCS/2 μM 2ME/5 ng/ml IL-3. Mouse NK cells (DX5^{+} cell) were positively isolated with MACS Beads (Miltenyi Biotec). Mouse BMDCs were prepared as previously reported (Akazawa et al., 2007a).

For purification of cells from spleen or LN, these tissues were treated with 400 IU MandleU/ml collagenase D (Roche) at 37°C for 25 min in HBSS (Sigma-Aldrich). Then EDTA was added, and the cell suspension was incubated for an additional 5 min at 37°C. After removal of RBC with ACK lysis buffer, splenocytes and LN cells were stained with CD45-FITC, CD3ε-PE, CD19-PE, DX5-PE, CD11b-FITC (eBioscience), and CD11c-FITC (BioLegend) and sorted by a FACSAria II (BD). The purity of sorted cells were >96%.

Construction and expression. Mouse INAM cDNA (A630077B13Rik) was obtained from RIKEN and placed into expression vector pEFBOS and pLenti-IRES-hrGFP, both of which provide the specialized components needed for expression of a recombinant C-terminal FLAG fusion (Akazawa et al., 2007a). For construction of shRNA-expressing lentivirus vector, The ClaI–XhoI fragment of pLenti6-blockit-dest (Invitrogen) was inserted into pLenti-IRES-hrGFP at the site of ClaI and XhoI. This vector was named pLenti-dest-IRES-hrGFP (pLDIG). INAM sequence 5′-CTTCTCTCCG-GTTAGTTATCT-3′ was targeted for INAM knockdown (shINAM/pLDIG) and 5′-AGTCTGACATACTTATACTTA-3′ was used for negative control (shCont/pLDIG). We used a gene-expression kit, Lentiviral system (Invitrogen), as previously described (Akazawa et al., 2007a). Four plasmids (one of the pLenti vectors, pLP1, pLP2, and pLP/VSVG) were transfected into 293 FT packaging cells, and the viral particles for transfection were prepared according to the manufacturer's protocol. The 100× concentrated virus particles were produced after centrifugation of 8,000 *g* at 4°C for 16 h. Lentivirus produced by pLenti-IRES-hrGFP and pLDIBG could be tittered by GFP expression using flow cytometry. Because the lentivirus vector pLenti-IRES-hrGFP has the IRES-GFP region, we prepared negative control virus by pLenti-IRES-hrGFP without construct. Infection efficiency for BMDC was high with the control vector compared with the INAM-expressing lentivector (Fig. S6 A).

Real-time PCR. BMDCs were harvested after 4 h of stimulation by 100 ng/ml LPS, 50 μg/ml polyI:C, 1 μg/ml Pam_3CSK_4 (Pam3), 100 nM mycoplasmal macrophage-activating lipopeptide-2 (Malp-2), 10 μg/ml CpG, and 2,000 IU/ml IFN-α (Ebihara et al., 2007). Mouse tissues (heart, stomach, small intestine, large intestine, lung, brain, muscle, liver, kidney, thymus, and spleen) were collected from C57BL/6. Splenocytes were stained with CD3-PE, CD19-PE, DX5-PE, CD11b-PE, CD11c-FITC, and PDCA1-PE (eBioscience) and sorted by FACSAria (BD). Purity was >98% in each population. For RNA extraction, we used the RNeasy kit (Invitrogen). After removal of genomic DNA by treatment with DNase, randomly primed cDNA strands were generated with Moloney mouse leukemia virus reverse transcription (Promega). RNA expression was quantified by quantitative RT-PCR with gene-specific primers (IL-15 forward, 5′-TTAACTGAGGCTGGCATTCATG-3′; IL-15 reverse, 5′-ACCTACACTGACACAGCCCAAA-3′; INAM forward, 5′-CAACTGCAATGCCACGCTA-3′; INAM reverse, 5′-TCCAACC-GAACACCTGAGACT-3′; β-actin forward, 5′-TTTGCAGCTCCTTC-GTTGC-3′; β-actin reverse, 5′-TCGTCATCCATGGCGAACT-3′; HPRT forward, 5′-GTTGGATACAGGCCAGACTTTGTTG-3′; and HPRT reverse, 5′-GAAGGGTAGGCTGGCCTATAGGCT-3′) and values were normalized to the expression of β-actin mRNA or HPRT mRNA.

Other primers for PCR were designed using Primer Express software (Applied Biosystems) for another experiment. The following primers were used for PCR: β-actin forward, 5′-CCTGGCACCCAGCACAAT-3′ and reverse, 5′-GCCGATCCACACGGAGTACT-3′; granzyme B forward, 5′-TCCTGCTACTGCTGACCTTGTC-3′ and reverse, 5′-ATGATCTC-CCCTGCCTTTGTC-3′; IFN-α4 forward, 5′-CTGCTGGCTGTGAG-GACATACT-3′ and reverse, 5′-AGGCACAGAGGCTGTGTTTCTT-3′; TRAIL (Tnfsf10) forward, 5′-CTTCACCAACGAGATGAAGCAG-3′ and reverse, 5′-TCCGTCTTTGAGAAGCAAGCTA-3′; and IL-12p40 (Il12b), forward, 5′-AATGTCTGCGTGCAAGCTCA-3′ and reverse, 5′-ATGCCCACTTGCTGCATGA-3′.

Anti-INAM pAb. C-terminal INAM (cINAM; 191–314 aa) was subcloned between the NdeI and SalI sites of pColdI vector (Takara Bio Inc.). 6× His-tagged cINAM protein was expressed in BL21 by manufacturer's methods. The cells were sonicated in 20 mM Tris-HCl, 150 mM NaCL, 1 mM PMSF, and 7 M Urea, pH 7.4, on ice. Expression products of cINAM were purified using the HisTrap HP kit (GE Healthcare). The extracted proteins were refolded by stepwise dialysis against decreasing amounts of urea. Rabbit anti-cINAM polyclonal Ab was produced with the cINAM proteins by standard protocol. IgG was purified by precipitation with 33% ammonium sulfate, dialyzed against PBS.

Surface labeling with biotin. Biotinylation of cell surface proteins was performed according to the reported method (Tsuji et al., 2001). In brief, ~10^8 cells were suspended in 1 ml Hepes-buffered saline (HBS), pH 8.5, and incubated with 10 ml of 10 mg/ml NHS-sulfobiotin (Vector Laboratories) for 1 h at room temperature. Cells were washed in HBS three times and then solubilized with lysis buffer containing 1% NP-40, pH 7.4. The cell lysate was immunoprecipitated with avidin-labeled Abs as described previously (Tsuji et al., 2001).

Immunoblot analysis. Lysates were harvested 24 h after transfection of Flag-tagged INAM/pEFBOS into 293FT cells and treated with *N*-glycosidase F

(PNGaseF; New England Biolabs, Inc.) by the manufacturer's method in some experiments. Protein samples were separated on SDS-PAGE and immunoblotted by anti-Flag M2 Ab (Sigma-Aldrich). In some experiments, we used highly purified rabbit anti–mouse INAM polyclonal Ab for immunoblotting. The anti-INAM IgG was further purified with protein A–Sepharose and absorbed with BL21 bacterial lysate (where the INAM immunogen was produced) that contained no INAM peptide.

Confocal microscopy. BMDCs and NK cells were infected with control or INAM-expressing lentivirus as described previously (Akazawa et al., 2007a). 24 h later, cells were fixed with 4% paraformaldehyde for 30 min and permeabilized with PBS containing 0.5% saponin for 30 min at room temperature. Fixed cells were stained with anti-FLAG mAb and Alexa Fluor 568–conjugated secondary Ab. Stable Ba/F3 transfectants expressing INAM were treated with Cytofix/Cytoperm (BD) according to the manufacturer. Then cells were stained with PE-phalloidin and rabbit anti-INAM pAb followed by Alexa Fluor 488–conjugated secondary Ab. Cells were analyzed on a confocal microscope (LSM 510 META; Carl Zeiss, Inc.) for the detection of INAM.

BMDC–NK interaction. BMDCs were co-cultured with freshly isolated NK cells (BMDC/NK = ~1:2–1:5) with or without 10 μg/ml polyI:C for 24 h (Akazawa et al., 2007a). In some experiments, function of BMDCs and NK cells was modified by lentivirus vector before BMDC/NK co-culture. IRF-3$^{-/-}$ BMDCs were transfected by control lentivirus and INAM-expressing lentivirus (INAM/pLenti-IRES-hrGFP) and incubated with 6 μg/ml polybrene for 24 h before co-culture. WT BMDCs were transfected with shRNA-expressing lentivirus (shCont/pLDIG or shINAM/pLDIG) and incubated with 6 μg/ml polybrene for 48 h before co-culture. Freshly isolated NK cells were transfected with control lentivirus and INAM-expressing lentivirus (INAM/pLenti-IRES-hrGFP) and cultured with 6 μg/ml polybrene in the presence of 500 IU/ml IL-2 for 72 h before co-culture. Activation of NK cells was assessed by concentration of IFN-γ (ELISA; GE Healthcare) in the medium and by NK cytotoxicity against B16D8. Cytotoxicity was determined by standard ^{51}Cr release assay as described previously (Akazawa et al., 2007a).

Ex vivo NK activation. Mice were i.p. injected with 250 μg polyI:C. After 24 h, spleen cells were harvested and then NK cells (DX5$^+$ cells) were positively isolated with the MACS system (Miltenyi Biotec). The DX5$^+$ NK cells were suspended in RPMI1640 with 10% FCS and mixed with ^{51}Cr-labeled B16D8 cells at indicated E/T ratios. After 4 h, supernatants were harvested and ^{51}Cr release was measured. Specific lysis was calculated by (specific release − spontaneous release)/(max release − spontaneous release). In some experiments, blood was drawn from the eyes of mice 8 h after polyI:C administration for cytokine measurement.

Test for in vivo NK activation in LN. 5 × 10^5 WT BMDCs incubated with or without 10 μg/ml polyI:C for 24 h or 5 × 10^5 IRF-3$^{-/-}$ BMDCs infected with control virus or INAM-expressing lentivirus and allowed to stand for 24 h were injected into the footpads of WT C57BL/6 mice. 48 h later, cells in their inguinal LN were harvested, stained with PE-DX5, and sorted by FACSAria II. RNA was extracted from the DX5-positive cells with TRIzol.

DC therapy. DC therapy against mice with B16D8 tumor burden was described previously (Akazawa et al., 2007a). C57BL/6 mice (n = 3) were shaved at the flank and injected s.c. with 6 × 10^5 syngeneic B16D8 melanoma cells (indicated as day 0). For DC therapy, BMDCs were prepared by transfecting control lentivirus or INAM-expressing lentivirus (INAM/pLenti-IRES-hrGFP) and cultured for 24 h. At the time point indicated in the figures, 10^6 BMDCs were injected s.c. near the tumor. To deplete NK cells in vivo, mice were i.p. injected with hybridoma ascites of anti-NK1.1 mAb (PK136; Akazawa et al., 2007a). Tumor volumes were measured using a caliper every 1 or 2 d. Tumor volume was calculated using the formula: tumor volume (cm^3) = (long diameter) × (short diameter) × (short diameter) × 0.4.

Statistical analysis. Statistical analyses were made with the Student's t test. The p-value of significant differences is reported.

Online supplemental material. TICAM-1–inducible genes encoding putative membrane proteins relevant for this study are summarized in Table S1. Fig. S1 shows KO mice results suggesting that both IPS-1 and TICAM-1 in BMDC participate in polyI:C-driven NK activation. Data presented in Fig. S2 characterizes the in vivo polyI:C response of INAM in LN cells. Figs. S3 and S4 demonstrate the properties of surface-expressed INAM analyzed by immunoprecipitation/blotting and confocal microscopy, respectively. Fig. S5 mentions the cytokine expression and maturation profiles of INAM-overexpressing BMDC. Fig. S6 shows the effect of gene silencing of INAM on the polyI:C-mediated cytokine-inducing profile in BMDC. Two pieces of data presented in Fig. S7 confirm the presence of the INAM protein in INAM lentivirus-transduced BMDCs and NK cells. Online supplemental material is available at http://www.jem.org/cgi/content/full/jem.20091573/DC1.

We thank Drs. T. Akazawa and N. Inoue (Osaka Medical Center for Cancer, Osaka, Japan) for their valuable discussions. Thanks are also due to many discussions by our laboratory members. Particularly, extensive English review by Dr. Hussein H. Aly is gratefully acknowledged.

This project was supported by Grants-in-Aid from the Ministry of Education, Science, and Culture and the Ministry of Health, Labor, and Welfare of Japan, Mitsubishi Foundation, Mochida Foundation, NorthTec Foundation Waxman Foundation, and Yakult Foundation.

The authors declare no financial or commercial conflict of interest.

Submitted: 20 July 2009
Accepted: 13 October 2010

REFERENCES

Akazawa, T., T. Ebihara, M. Okuno, Y. Okuda, M. Shingai, K. Tsujimura, T. Takahashi, M. Ikawa, M. Okabe, N. Inoue, et al. 2007a. Antitumor NK activation induced by the Toll-like receptor 3-TICAM-1 (TRIF) pathway in myeloid dendritic cells. *Proc. Natl. Acad. Sci. USA.* 104:252–257. doi:10.1073/pnas.0605978104

Akazawa, T., M. Shingai, M. Sasai, T. Ebihara, N. Inoue, M. Matsumoto, and T. Seya. 2007b. Tumor immunotherapy using bone marrow-derived dendritic cells overexpressing Toll-like receptor adaptors. *FEBS Lett.* 581:3334–3340. doi:10.1016/j.febslet.2007.06.019

Azuma, M., R. Sawahata, Y. Akao, T. Ebihara, S. Yamazaki, M. Matsumoto, M. Hashimoto, K. Fukase, Y. Fujimoto, and T. Seya. 2010. The peptide sequence of diacyl lipopeptides determines dendritic cell TLR2-mediated NK activation. *PLoS One.* 5:e12550. doi:10.1371/journal.pone.0012550

Bertram, L., B.M. Schjeide, B. Hooli, K. Mullin, M. Hiltunen, H. Soininen, M. Ingelsson, L. Lannfelt, D. Blacker, and R.E. Tanzi. 2008. No association between CALHM1 and Alzheimer's disease risk. *Cell.* 135:993–994, author reply :994–996. doi:10.1016/j.cell.2008.11.030

Brandt, C.S., M. Baratin, E.C. Yi, J. Kennedy, Z. Gao, B. Fox, B. Haldeman, C.D. Ostrander, T. Kaifu, C. Chabannon, et al. 2009. The B7 family member B7-H6 is a tumor cell ligand for the activating natural killer cell receptor NKp30 in humans. *J. Exp. Med.* 206:1495–1503. doi:10.1084/jem.20090681

Brilot, F., T. Strowig, S.M. Roberts, F. Arrey, and C. Münz. 2007. NK cell survival mediated through the regulatory synapse with human DCs requires IL-15Ralpha. *J. Clin. Invest.* 117:3316–3329. doi:10.1172/JCI31751

Cerwenka, A., and L.L. Lanier. 2001. Natural killer cells, viruses and cancer. *Nat. Rev. Immunol.* 1:41–49. doi:10.1038/35095564

Cerwenka, A., A.B. Bakker, T. McClanahan, J. Wagner, J. Wu, J.H. Phillips, and L.L. Lanier. 2000. Retinoic acid early inducible genes define a ligand family for the activating NKG2D receptor in mice. *Immunity.* 12:721–727. doi:10.1016/S1074-7613(00)80222-8

Cerwenka, A., J.L. Baron, and L.L. Lanier. 2001. Ectopic expression of retinoic acid early inducible-1 gene (RAE-1) permits natural killer cell-mediated rejection of a MHC class I-bearing tumor in vivo. *Proc. Natl. Acad. Sci. USA.* 98:11521–11526. doi:10.1073/pnas.201238598

Dreses-Werringloer, U., J.C. Lambert, V. Vingtdeux, H. Zhao, H. Vais, A. Siebert, A. Jain, J. Koppel, A. Rovelet-Lecrux, D. Hannequin, et al. 2008. A polymorphism in CALHM1 influences Ca2+ homeostasis,

Abeta levels, and Alzheimer's disease risk. *Cell.* 133:1149–1161. doi:10.1016/j.cell.2008.05.048

Ebihara, T., H. Masuda, T. Akazawa, M. Shingai, H. Kikuta, T. Ariga, M. Matsumoto, and T. Seya. 2007. Induction of NKG2D ligands on human dendritic cells by TLR ligand stimulation and RNA virus infection. *Int. Immunol.* 19:1145–1155. doi:10.1093/intimm/dxm073

Fernandez, N.C., A. Lozier, C. Flament, P. Ricciardi-Castagnoli, D. Bellet, M. Suter, M. Perricaudet, T. Tursz, E. Maraskovsky, and L. Zitvogel. 1999. Dendritic cells directly trigger NK cell functions: cross-talk relevant in innate anti-tumor immune responses in vivo. *Nat. Med.* 5:405–411. doi:10.1038/7403

Fitzgerald, K.A., S.M. McWhirter, K.L. Faia, D.C. Rowe, E. Latz, D.T. Golenbock, A.J. Coyle, S.M. Liao, and T. Maniatis. 2003. IKKepsilon and TBK1 are essential components of the IRF3 signaling pathway. *Nat. Immunol.* 4:491–496. doi:10.1038/ni921

Gerosa, F., B. Baldani-Guerra, C. Nisii, V. Marchesini, G. Carra, and G. Trinchieri. 2002. Reciprocal activating interaction between natural killer cells and dendritic cells. *J. Exp. Med.* 195:327–333. doi:10.1084/jem.20010938

Hamerman, J.A., K. Ogasawara, and L.L. Lanier. 2004. Cutting edge: Toll-like receptor signaling in macrophages induces ligands for the NKG2D receptor. *J. Immunol.* 172:2001–2005.

Honda, K., H. Yanai, H. Negishi, M. Asagiri, M. Sato, T. Mizutani, N. Shimada, Y. Ohba, A. Takaoka, N. Yoshida, and T. Taniguchi. 2005. IRF-7 is the master regulator of type-I interferon-dependent immune responses. *Nature.* 434:772–777. doi:10.1038/nature03464

Hornung, V., S. Rothenfusser, S. Britsch, A. Krug, B. Jahrsdörfer, T. Giese, S. Endres, and G. Hartmann. 2002. Quantitative expression of toll-like receptor 1-10 mRNA in cellular subsets of human peripheral blood mononuclear cells and sensitivity to CpG oligodeoxynucleotides. *J. Immunol.* 168:4531–4537.

Huntington, N.D., N. Legrand, N.L. Alves, B. Jaron, K. Weijer, A. Plet, E. Corcuff, E. Mortier, Y. Jacques, H. Spits, and J.P. Di Santo. 2009. IL-15 trans-presentation promotes human NK cell development and differentiation in vivo. *J. Exp. Med.* 206:25–34. doi:10.1084/jem.20082013

Iwasaki, A., and R. Medzhitov. 2004. Toll-like receptor control of the adaptive immune responses. *Nat. Immunol.* 5:987–995. doi:10.1038/ni1112

Kalinski, P., R.B. Mailliard, A. Giermasz, H.J. Zeh, P. Basse, D.L. Bartlett, J.M. Kirkwood, M.T. Lotze, and R.B. Herberman. 2005. Natural killer-dendritic cell cross-talk in cancer immunotherapy. *Expert Opin. Biol. Ther.* 5:1303–1315. doi:10.1517/14712598.5.10.1303

Kato, H., O. Takeuchi, S. Sato, M. Yoneyama, M. Yamamoto, K. Matsui, S. Uematsu, A. Jung, T. Kawai, K.J. Ishii, et al. 2006. Differential roles of MDA5 and RIG-I helicases in the recognition of RNA viruses. *Nature.* 441:101–105. doi:10.1038/nature04734

Kawai, T., K. Takahashi, S. Sato, C. Coban, H. Kumar, H. Kato, K.J. Ishii, O. Takeuchi, and S. Akira. 2005. IPS-1, an adaptor triggering RIG-I- and Mda5-mediated type I interferon induction. *Nat. Immunol.* 6:981–988. doi:10.1038/ni1243

Kubin, M.Z., D.L. Parshley, W. Din, J.Y. Waugh, T. Davis-Smith, C.A. Smith, B.M. Macduff, R.J. Armitage, W. Chin, L. Cassiano, et al. 1999. Molecular cloning and biological characterization of NK cell activation-inducing ligand, a counterstructure for CD48. *Eur. J. Immunol.* 29:3466–3477. doi:10.1002/(SICI)1521-4141(199911)29:11<3466::AID-IMMU3466>3.0.CO;2-9

Lee, A.E., L.A. Rogers, J.M. Longcroft, and R.E. Jeffery. 1990. Reduction of metastasis in a murine mammary tumour model by heparin and polyinosinic-polycytidylic acid. *Clin. Exp. Metastasis.* 8:165–171. doi:10.1007/BF00117789

Levy, S., and T. Shoham. 2005. The tetraspanin web modulates immune-signalling complexes. *Nat. Rev. Immunol.* 5:136–148. doi:10.1038/nri1548

Lucas, M., W. Schachterle, K. Oberle, P. Aichele, and A. Diefenbach. 2007. Dendritic cells prime natural killer cells by trans-presenting interleukin 15. *Immunity.* 26:503–517. doi:10.1016/j.immuni.2007.03.006

Masuda, H., Y. Saeki, M. Nomura, K. Shida, M. Matsumoto, M. Ui, L.L. Lanier, and T. Seya. 2002. High levels of RAE-1 isoforms on mouse tumor cell lines assessed by anti-"pan" RAE-1 antibody confer tumor susceptibility to NK cells. *Biochem. Biophys. Res. Commun.* 290:140–145. doi:10.1006/bbrc.2001.6165

Matsumoto, M., and T. Seya. 2008. TLR3: interferon induction by double-stranded RNA including poly(I:C). *Adv. Drug Deliv. Rev.* 60:805–812. doi:10.1016/j.addr.2007.11.005

McCartney, S., W. Vermi, S. Gilfillan, M. Cella, T.L. Murphy, R.D. Schreiber, K.M. Murphy, and M. Colonna. 2009. Distinct and complementary functions of MDA5 and TLR3 in poly(I:C)-mediated activation of mouse NK cells. *J. Exp. Med.* 206:2967–2976. doi:10.1084/jem.20091181

Medzhitov, R., and C.A. Janeway Jr. 1997. Innate immunity: the virtues of a nonclonal system of recognition. *Cell.* 91:295–298. doi:10.1016/S0092-8674(00)80412-2

Meylan, E., J. Curran, K. Hofmann, D. Moradpour, M. Binder, R. Bartenschlager, and J. Tschopp. 2005. Cardif is an adaptor protein in the RIG-I antiviral pathway and is targeted by hepatitis C virus. *Nature.* 437:1167–1172. doi:10.1038/nature04193

Miyake, T., Y. Kumagai, H. Kato, Z. Guo, K. Matsushita, T. Satoh, T. Kawagoe, H. Kumar, M.H. Jang, T. Kawai, et al. 2009. Poly I:C-induced activation of NK cells by CD8 alpha+ dendritic cells via the IPS-1 and TRIF-dependent pathways. *J. Immunol.* 183:2522–2528. doi:10.4049/jimmunol.0901500

Mukai, M., F. Imamura, M. Ayaki, K. Shinkai, T. Iwasaki, K. Murakami-Murofushi, H. Murofushi, S. Kobayashi, T. Yamamoto, H. Nakamura, and H. Akedo. 1999. Inhibition of tumor invasion and metastasis by a novel lysophosphatidic acid (cyclic LPA). *Int. J. Cancer.* 81:918–922. doi:10.1002/(SICI)1097-0215(19990611)81:6<918::AID-IJC13>3.0.CO;2-E

Newman, K.C., and E.M. Riley. 2007. Whatever turns you on: accessory-cell-dependent activation of NK cells by pathogens. *Nat. Rev. Immunol.* 7:279–291. doi:10.1038/nri2057

Nomura, M., Z. Zou, T. Joh, Y. Takihara, Y. Matsuda, and K. Shimada. 1996. Genomic structures and characterization of Rae1 family members encoding GPI-anchored cell surface proteins and expressed predominantly in embryonic mouse brain. *J. Biochem.* 120:987–995.

Ohteki, T., H. Tada, K. Ishida, T. Sato, C. Maki, T. Yamada, J. Hamuro, and S. Koyasu. 2006. Essential roles of DC-derived IL-15 as a mediator of inflammatory responses in vivo. *J. Exp. Med.* 203:2329–2338. doi:10.1084/jem.20061297

Oshiumi, H., M. Matsumoto, K. Funami, T. Akazawa, and T. Seya. 2003a. TICAM-1, an adaptor molecule that participates in Toll-like receptor 3-mediated interferon-beta induction. *Nat. Immunol.* 4:161–167. doi:10.1038/ni886

Oshiumi, H., M. Sasai, K. Shida, T. Fujita, M. Matsumoto, and T. Seya. 2003b. TIR-containing adapter molecule (TICAM)-2, a bridging adapter recruiting to toll-like receptor 4 TICAM-1 that induces interferon-beta. *J. Biol. Chem.* 278:49751–49762. doi:10.1074/jbc.M305820200

Sasai, M., M. Shingai, K. Funami, M. Yoneyama, T. Fujita, M. Matsumoto, and T. Seya. 2006. NAK-associated protein 1 participates in both the TLR3 and the cytoplasmic pathways in type I IFN induction. *J. Immunol.* 177:8676–8683.

Sato, M., H. Suemori, N. Hata, M. Asagiri, K. Ogasawara, K. Nakao, T. Nakaya, M. Katsuki, S. Noguchi, N. Tanaka, and T. Taniguchi. 2000. Distinct and essential roles of transcription factors IRF-3 and IRF-7 in response to viruses for IFN-alpha/beta gene induction. *Immunity.* 13:539–548. doi:10.1016/S1074-7613(00)00053-4

Seth, R.B., L. Sun, C.K. Ea, and Z.J. Chen. 2005. Identification and characterization of MAVS, a mitochondrial antiviral signaling protein that activates NF-kappaB and IRF 3. *Cell.* 122:669–682. doi:10.1016/j.cell.2005.08.012

Seya, T., and M. Matsumoto. 2009. The extrinsic RNA-sensing pathway for adjuvant immunotherapy of cancer. *Cancer Immunol. Immunother.* 58:1175–1184. doi:10.1007/s00262-008-0652-9

Sivori, S., M. Falco, M. Della Chiesa, S. Carlomagno, M. Vitale, L. Moretta, and A. Moretta. 2004. CpG and double-stranded RNA trigger human NK cells by Toll-like receptors: induction of cytokine release and cytotoxicity against tumors and dendritic cells. *Proc. Natl. Acad. Sci. USA.* 101:10116–10121. doi:10.1073/pnas.0403744101

Tanaka, H., Y. Mori, H. Ishii, and H. Akedo. 1988. Enhancement of metastatic capacity of fibroblast-tumor cell interaction in mice. *Cancer Res.* 48:1456–1459.

Tsuji, S., J. Uehori, M. Matsumoto, Y. Suzuki, A. Matsuhisa, K. Toyoshima, and T. Seya. 2001. Human intelectin is a novel soluble lectin that recognizes galactofuranose in carbohydrate chains of bacterial cell wall. *J. Biol. Chem.* 276:23456–23463. doi:10.1074/jbc.M103162200

Vivier, E., E. Tomasello, M. Baratin, T. Walzer, and S. Ugolini. 2008. Functions of natural killer cells. *Nat. Immunol.* 9:503–510. doi:10.1038/ni1582

Xu, L.G., Y.Y. Wang, K.J. Han, L.Y. Li, Z. Zhai, and H.B. Shu. 2005. VISA is an adapter protein required for virus-triggered IFN-beta signaling. *Mol. Cell.* 19:727–740. doi:10.1016/j.molcel.2005.08.014

Yamamoto, M., S. Sato, H. Hemmi, K. Hoshino, T. Kaisho, H. Sanjo, O. Takeuchi, M. Sugiyama, M. Okabe, K. Takeda, and S. Akira. 2003a. Role of adaptor TRIF in the MyD88-independent toll-like receptor signaling pathway. *Science.* 301:640–643. doi:10.1126/science.1087262

Yamamoto, M., S. Sato, H. Hemmi, S. Uematsu, K. Hoshino, T. Kaisho, O. Takeuchi, K. Takeda, and S. Akira. 2003b. TRAM is specifically involved in the Toll-like receptor 4-mediated MyD88-independent signaling pathway. *Nat. Immunol.* 4:1144–1150. doi:10.1038/ni986

Yoneyama, M., M. Kikuchi, T. Natsukawa, N. Shinobu, T. Imaizumi, M. Miyagishi, K. Taira, S. Akira, and T. Fujita. 2004. The RNA helicase RIG-I has an essential function in double-stranded RNA-induced innate antiviral responses. *Nat. Immunol.* 5:730–737. doi:10.1038/ni1087

Zanoni, I., M. Foti, P. Ricciardi-Castagnoli, and F. Granucci. 2005. TLR-dependent activation stimuli associated with Th1 responses confer NK cell stimulatory capacity to mouse dendritic cells. *J. Immunol.* 175:286–292.

Zou, Z., M. Nomura, Y. Takihara, T. Yasunaga, and K. Shimada. 1996. Isolation and characterization of retinoic acid-inducible cDNA clones in F9 cells: a novel cDNA family encodes cell surface proteins sharing partial homology with MHC class I molecules. *J. Biochem.* 119:319–328.

Published November 8, 2010

JEM

SUPPLEMENTAL MATERIAL

Ebihara et al., http://www.jem.org/cgi/content/full/jem.20091573/DC1

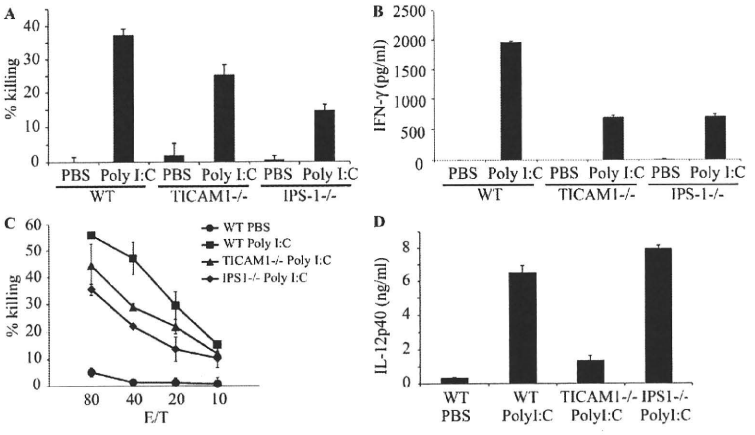

Figure S1. KO mice results suggest that both IPS-1 and TICAM-1 in BMDC participate in polyI:C-driven NK activation. (A and B) IPS-1 and TICAM-1 in BMDC participate in polyI:C-driven NK activation. 2.5 × 10^5 BMDCs prepared from WT, TICAM1$^{-/-}$, and IPS1$^{-/-}$ mice were incubated with 5 × 10^5 NK cells in the presence or absence (PBS) of 50 µg/ml polyI:C for 24 h. Then, the supernatants were harvested for IFN-γ ELISA (B). To determine NK cytotoxicity, ^{51}Cr-labeled B16D8 cells were added to the culture and, 4 h later, released ^{51}Cr was measured (A). One representative of three similar experiments is shown. (C) Both IPS-1 and TICAM-1 participate in in vivo polyI:C-induced NK activation. WT, IPS-1$^{-/-}$, and TICAM-1$^{-/-}$ mice were i.p. injected with 250 µg polyI:C. After 24 h, NK cells were harvested by DX5-MACS beads from spleen and used as effector cells in a cytotoxic assay with ^{51}Cr-labeled B16D8 targets. Cytotoxic activity of NK cells was measured under the indicated E/T ratios 4 h after the E/T mixing. One representative of the three similar experiments is shown. (D) Increasing serum level of IL-12p40 is dependent on TICAM-1. 250 µg polyI:C was i.p. injected into a series of mice as in B. 8 h after injection of polyI:C, blood serum was collected to determine the levels of IL-12p40 by ELISA. Although it is not depicted, IL-12p70 was not detected in these samples by ELISA. Data in A–D represent mean ± SD.

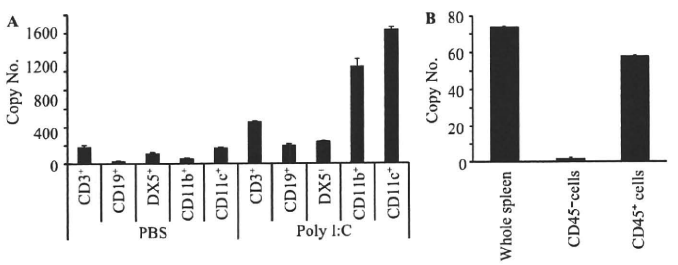

Figure S2. In vivo polyI:C response of INAM in LN cells. (A) Up-regulation of INAM expression in LN cells by polyI:C injection. WT C57BL/6 mice were i.p. injected with 100 µg polyI:C or control buffer. After 24 h, inguinal, axillary, and mesenteric LN were harvested. Cell populations with indicated markers were separated by FACS sorting, and the INAM mRNA level of each population was determined by real-time PCR. (B) CD45$^+$ cells express INAM. Splenocytes were separated into CD45$^-$ and CD45$^+$ cells after the polyI:C injection as in A. The INAM mRNA levels of the two populations were determined by real-time PCR. Representative data from one of three experiments are shown. Data in A and B represent mean ± SD.

Published November 8, 2010

JEM

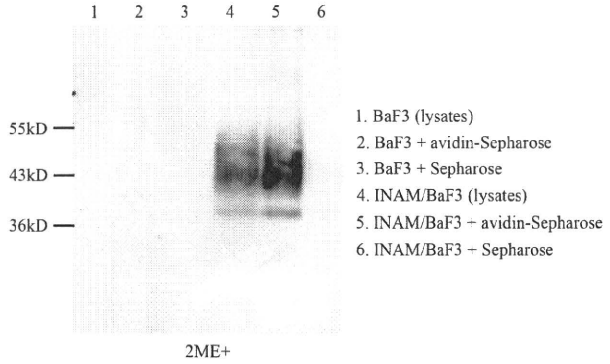

Figure S3. INAM is expressed on cell surface. Membrane proteins of Flag-tagged INAM-expressing BaF3 (INAM/BaF3) and control BaF3 were biotinylated and solubilized. Biotinylated proteins were immunoprecipitated by Avidin-Sepharose or control Sepharose. After electrophoresis on SDS-PAGE, INAM was detected by anti-Flag M2 mAb.

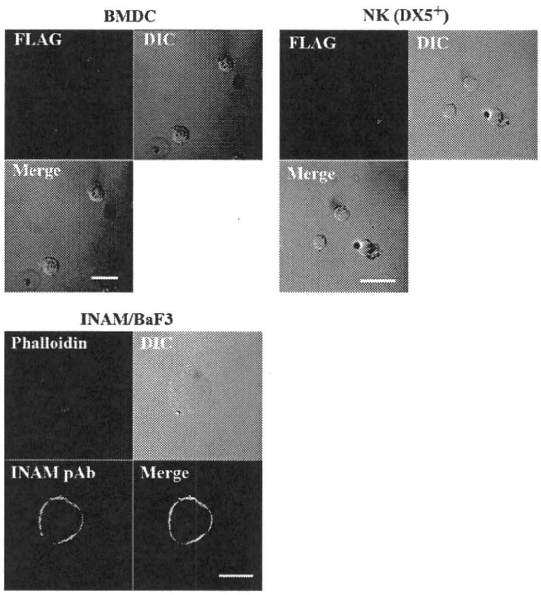

Figure S4. Confocal analysis of surface-expressed INAM. WT BMDC (left) or NK cells (right) were infected with INAM-expressing vector and stained with anti-FLAG mAb (Alexa Fluor 568). Stable Ba/F3 transfectants expressing INAM (bottom) were permeabilized and stained with phalloidin and anti-INAM pAb, followed by Alexa Fluor 488–conjugated secondary antibody. Cells were analyzed on a confocal laser-scanning microscope (LSM 510 META). Bars, 20 μm.

Published November 8, 2010

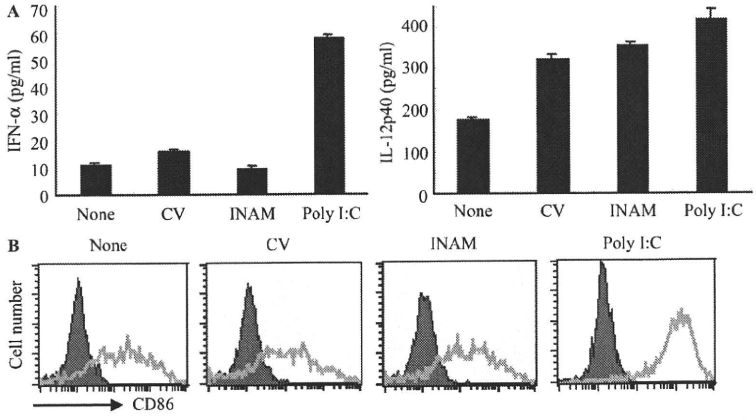

Figure S5. INAM-overexpressing BMDC did not induce cytokine responses and maturation. WT BMDCs were transfected with control lentivirus (CV) or INAM-expressing lentivirus (INAM-virus) and cultured for 24 h. (A) ELISA of IFN-α and IL-12p40 in the culture supernatants. Data shown are means ± SD of triplicate samples from one experiment representative of three. (B) Flow cytometry for CD86 in the transfected BMDC. Poly I:C stimulation (10 μg/ml) was used for positive control.

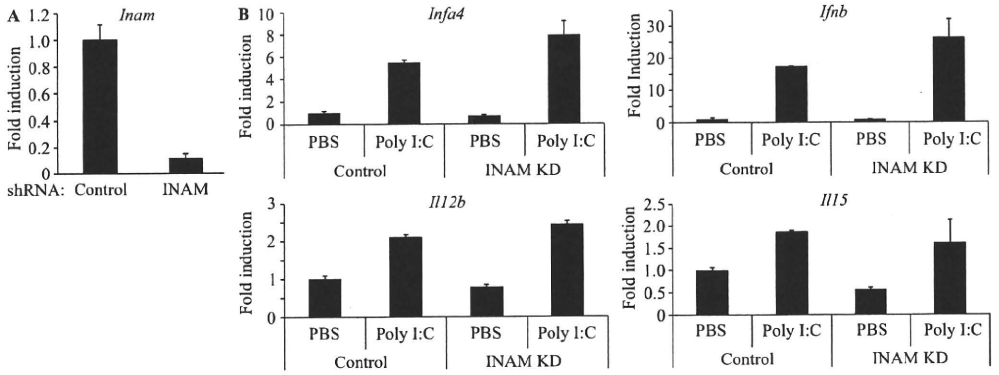

Figure S6. The effect of gene silencing of INAM on the polyI:C-mediated cytokine inducing profile in BMDC. (A) Gene silencing of INAM in BMDC. 5 × 10^5 WT BMDCs were infected with INAM shRNA-generating lentivirus or control lentivirus. After 36 h, the levels of INAM mRNA expression were assessed by real time PCR. Data show one of three similar experiments. (B) Effect of BMDC INAM on cytokine expression. INAM in 5 × 10^5 WT BMDCs was silenced as in A. Then, control or INAM-silenced BMDC were stimulated with 10 μg/ml polyI:C for 8 h. RNA was harvested from BMDC with RNeasy and the levels of indicated mRNA were determined by real-time PCR. Data show one of two similar experimental results. Data in A and B represent mean ± SD.

Published November 8, 2010

JEM

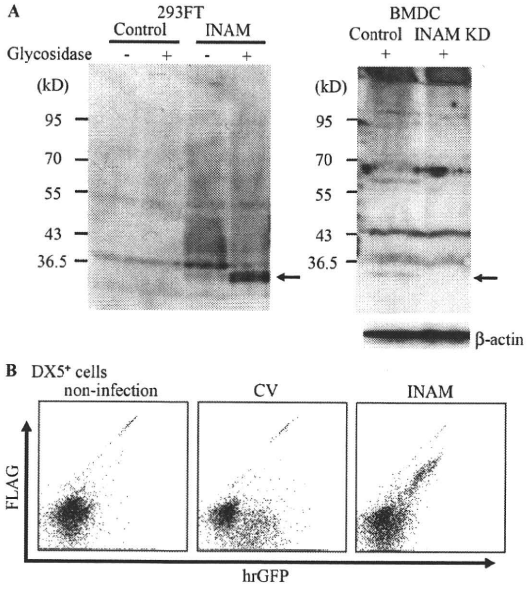

Figure S7. Detection of the INAM protein in DCs and NK cells. (A) Detection of the endogenous INAM protein in BMDC. 5 × 10^6 BMDCs were transduced with INAM-shRNA or control shRNA–expressing lentivirus. 48 h later, these cells were lysed and treated with *N*-glycosidase F for 2 h at 37°C. All cell lysates were subjected to SDS-PAGE and immunoblotted by rabbit anti-INAM pAb. The cell lysates from 293FT cells transfected with pEFBOS or pEFBOS/INAM were used as negative and positive control, respectively. Arrows indicate the band for INAM. Mr markers are shown to the left. One of three similar experiments is shown. (B) DX5+ NK cells express GFP and FLAG, markers for INAM. 5 × 10^5 DX5+ cells were transduced with control or INAM-expressing lentivirus for 48 h. Then, these cells were permeabilized and stained with rabbit anti-FLAG pAb and PE-anti rabbit IgG. Levels of FLAG and hrGFP, reflecting INAM expression, were measured by FACSCalibur. Experiments were performed more than six times with different conditions and representative data are shown.

Table S1. TICAM-1-inducible genes encoding putative membrane or GPI-anchored proteins

Official symbol	Other aliases	UniGene ID	Fold induction (poly I:C stimulation/nonstimulation)			
			WT	MyD88$^{-/-}$	TLR3$^{-/-}$	TICAM-1$^{-/-}$
Aplnr	APJ, Agtrl1, msr/apj	Mm.29368	2.074101377	0.79485698	0.24913528	0.296911294
Fam26f	INAM, A630077B13Rik	Mm.34479	15.57360865	8.048081457	0.939239821	1.221297574
Clec4e	Clecsf9, Mincle	Mm.248327	5.65851862	7.142025946	2.761541794	2.087684899
Ly6i	Ly-6M, AI789751	Mm.358339	5.679941154	26.36364231	0.734513568	1.09611157
Slamf8	Blame, SBBI42	Mm.179812	6.814581008	5.127202394	1.802731559	1.122849288
Tmem171	Gm905, MGC117733	Mm.28264	12.42279971	7.454421156	2.274145126	3.051240138
Pvrl4	1200017F15Rik, Prr4	Mm.263414	5.02297837	4.096701442	1.627391239	1.961829994
Vcam1	CD106	Mm.76649	4.742423155	4.572993249	0.948952117	0.554171652
Tnfsf10	APO-2L, TL2, Trail	Mm.1062	41.9745751	30.22262268	6.007858781	2.631939934

Cancer Science
The official journal of the Japanese Cancer Association

Adjuvant engineering for cancer immunotherapy: Development of a synthetic TLR2 ligand with increased cell adhesion

Takashi Akazawa,[1,2,5] Norimitsu Inoue,[1] Hiroaki Shime,[1,3] Ken Kodama,[4] Misako Matsumoto[2,3] and Tsukasa Seya[2,3]

Departments of [1]Molecular Genetics, [2]Immunology, Osaka Medical Center for Cancer and Cardiovascular Diseases, Osaka; [3]Department of Microbiology and Immunology, Hokkaido University Graduate School of Medicine, Sapporo; [4]Department of Surgery, Osaka Medical Center for Cancer and Cardiovascular Diseases, Osaka, Japan

(Recieved August 21, 2009/Revised December 8, 2009; March 23, 2010/Accepted March 28, 2010/Accepted manuscript online April 5, 2010/Article first published online May 7, 2010)

The development of effective immunoadjuvants for tumor immunotherapy is of fundamental importance. The use of *Mycobacterium bovis* bacillus Calmette-Guérin cell wall skeleton (BCG-CWS) in tumor immunotherapy has been examined in various clinical applications. Because BCG-CWS is a macromolecule that cannot be chemically synthesized, the development of an alternative synthetic molecule is necessary to ensure a constant supply of adjuvant. In the present study, a new adjuvant was designed based on the structure of macrophage-activating lipopeptide (MALP)-2, which is a Toll-like receptor (TLR)-2 ligand similar to BCG-CWS. Macrophage-activating lipopeptide-2, [S-(2,3-bispalmitoyloxypropyl)Cys (P2C) – GNNDESNISFKEK], originally identified in a Mycoplasma species, is a lipopeptide that can be chemically synthesized. A MALP-2 peptide was substituted with a functional motif, RGDS, creating a novel molecule named P2C-RGDS. RGDS was selected because its sequence constitutes an integrin-binding motif and various integrins are expressed in immune cells including dendritic cells (DCs). Thus, this motif adds functionality to the ligand. P2C-RGDS activated DCs and splenocytes more efficiently than MALP-2 over short incubation times *in vitro*, and the RGDS motif contributed to their activation. Furthermore, P2C-RGDS showed higher activity than MALP-2 in inducing migration of DCs to draining lymph node, and in inhibiting tumor growth *in vivo*. This process of designing and developing synthetic adjuvants has been named "adjuvant engineering," and the evaluation and improvement of P2C-RGDS constitutes a first step in the development of stronger synthetic adjuvants in the future. (*Cancer Sci* 2010; 101: 1596–1603)

Bacterial adjuvants that were used as biological response modifiers (BRM) for cancer immunotherapy in the 1970s have recently been re-evaluated.[1–3] Cancer antigens that had been identified in many laboratories were tested as peptide vaccines for clinical applications, but the peptides alone were not sufficient to fully activate the immune system.[4] These results suggested that the activation of the innate immune system, including dendritic cells (DCs), by a supporting adjuvant was important.[5–8] In peptide vaccine therapy, the T cells of the acquired immune system play an important role in recognizing and attacking tumor cells.[9] Dendritic cells play a key role in the regulation of the acquired immune system by presenting antigen and inducing a primary immune response. The identification of the Toll-like receptor (TLR) family advanced the understanding of DC function and of the role of adjuvants, because almost all microbial adjuvants work as TLR ligands and activate DCs.[10–12] These findings provide the basis for the understanding of the mechanism of adjuvant therapy.

Dr Azuma developed BCG-CWS, a cell-wall skeleton preparation of *Mycobacterium bovis* bacillus Calmette-Guérin,[13,14] as an antitumor immunotherapeutic adjuvant. Although many BRM studies have been discontinued, basic and clinical research on BCG-CWS has continued at Osaka Medical Center for Cancer. We reported that BCG-CWS is a ligand of TLR2/4[15–17] and acts as an effective adjuvant to induce CTLs in irradiated tumors in a mouse experimental model. These activities are mediated by the myeloid differentiation protein 88 (MyD88),[18] which is a TLR adaptor molecule. The effectiveness of BCG-CWS in improving the prognosis for cancer patients after surgery was confirmed through clinical research.[19]

Interleukin (IL)-23 and interferon (IFN)-γ are the main cytokines induced by BCG-CWS *in vivo*[14,19,20] and are important for antitumor immunity.[21,22] Interleukin-12 is well known as an antitumor cytokine,[23] and IL-23 shares the IL12p40 subunit with IL-12.[22] Unexpectedly, IL-23 advanced tumor growth in experiments with IL-23R$^{-/-}$ mice or neutralizing antibodies by interacting with Th17 cells.[24–26] However, systemic administration of IL-23 was also reported to have antitumor effects similar to those of IL-12,[27] and TLR2 ligands exhibit antitumor activity[28–30] that may be mediated by the induction of IL-23.

Although BCG-CWS is effective as an adjuvant, its clinical use is limited in purity, stability, and a stable supply because it cannot be chemically synthesized and is therefore prepared from bacterial cells. These factors indicate that there is a need to develop new synthetic adjuvants as effective as BCG-CWS. The present report describes the design of such adjuvants based on the structure of the TLR2 ligand and in consideration of the need for IL-23 induction. Macrophage-activating lipopeptide (MALP)-2, a lipopeptide of mycoplasmic origin, is a TLR2 ligand that can be chemically synthesized. No functional consensus peptide sequences were identified in MALP-2. The N-terminal cysteine of the 13-amino-acid peptide of bacterial origin was modified with 2 palmitates [Pam2Cys or P2C, S-(2,3-bispalmitoyloxypropyl)-cysteine],[31] but P2C alone does not work as a TLR2 ligand.[32] Bacterial and synthetic TLR2 ligands (MALP-2, FSL-1,[32] P2C-SKKKK[33]) contain mostly hydrophilic peptides, and the presence of solubilizers critically affects their TLR2 agonistic ability,[34] suggesting that the activity of compounds as TLR2 agonists correlates with their solubility.

CD11c is a member of the integrin superfamily and is known to be a marker of DCs.[35] Dendritic cells also express other integrin molecules such as $\alpha V/\beta 3$ and $\alpha 5/\beta 1$, and the RGDS motif specifically binds to these integrins.[36,37] Virus particles expressing proteins containing the RGD motif efficiently infect DCs.[37] Therefore, a new TLR2 ligand was developed by

[5]To whom correspondence should be addressed.
E-mail: akazawa-ta@mc.pref.osaka.jp

doi: 10.1111/j.1349-7006.2010.01583.x

replacing the peptide of bacterial origin with a hydrophilic functional motif (adjuvant engineering). P2C and the RGDS peptide were linked to increase the efficiency of ligand adherence to DCs or other immune cells, and the effect of the new adjuvant on antitumor activities *in vitro* and *in vivo* was examined.

Materials and Methods

Mice, cells, and reagents. Toll/IL-1 receptor homology-containing adaptor molecule (TICAM)-$1^{-/-}$ mice were generated in our laboratory.[2] Toll-like receptor (TLR)-$2^{-/-}$ and MyD88$^{-/-}$ mice were provided by Shizuo Akira (Osaka University).[38] The mice were maintained under specific pathogen-free conditions in the animal facility of the Osaka Medical Center. They were backcrossed with C57BL/6 mice >8 times before use. Wild-type (WT) C57BL/6 mice were purchased from Japan Clea (Tokyo, Japan). All animal experiments were approved by the committee at Osaka Medical Center for Cancer. EG7 cells are ovalbumin-transfected EL4 and were obtained from the American Type Culture Collection (ATCC, Manassas, VA, USA).[39] B16D8 was established in our laboratory as a subline of the B16 melanoma cell line.[18] Cell lysates were prepared by the freeze-thaw method.

Preparation of mouse bone marrow-derived DCs (BMDCs), splenocytes, and lymph node cells. Bone marrow-derived DCs were prepared as previously described[35,40] with minor modifications, and were cultured in RPMI-1640 (Invitrogen, Carlsbad, CA, USA) containing 10 ng/mL mouse granulocyte-macrophage colony-stimulating factor (PeproTech EC, London, UK), 50 μM 2-mercaptoethanol (Invitrogen), 10 mM HEPES, and 10% FCS (Bio Whittaker, Walkersville, MD, USA). The inguinal lymph node cells and splenocytes were prepared by using Lympholyte-M (Cedarlane, Burlington, ON, Canada). CD11c-positive and -negative cells, and CD90-positive and -negative cells were separated from splenocytes by using CD11c or CD90 microbeads (Miltenyi Biotec, Auburn, CA, USA).

***In vitro* assay.** For the simple stimulation assay *in vitro*, BMDCs or splenocytes were cultured with 10 μg/mL of BCG-CWS,[18] 100 nM of MALP-2 and the designed lipopeptide (purity >90%; Biologica, Aichi, Japan) for 24 h (BMDCs, FACS), 48 h (BMDCs, ELISA), or 72 h (splenocytes, ELISA). For the inhibition assay, BMDCs or splenocytes were pre-incubated with the indicated concentrations of RGDS peptide or anti-CD29 antibody (eBioscience, San Diego, CA, USA) at 4°C for 30 min before stimulating them with TLR2 ligands at 4°C for 60 min. The cells were then washed and re-cultured for 48 h (BMDCs, ELISA) or 72 h (splenocytes, ELISA). The Mixed Lymphocyte Reaction (MLR) assay was performed as previously described,[40] and the results were analyzed as uptake of [^{3}H]thymidine (1 μCi/well; Amersham Biosciences, Piscataway, NJ, USA). Bone marrow-derived DCs stimulated with TLR2 ligands for 24 h (C57BL/6, 5×10^4 cells) were co-cultured with CD90-positive T cells (BALB/c, 10^5 cells) for 72 h. To exclude the possible effect of contaminating lipopolysaccharide, lipopeptides were pretreated with polymyxin B (Sigma-Aldrich, St. Louis, MO, USA) at 37°C for 60 min.

Fluorescence-activated cell sorter (FACS) analysis, intracellular cytokine staining, and ELISA. For FACS analysis, cells were suspended in PBS containing 0.1% sodium azide and 1% FCS, and then incubated for 30 min at 4°C with FITC-conjugated anti-mouse CD80, antimouse CD86, antimouse CD8, or isotype control antibody; or with phycoerythrin-conjugated antimouse CD4 or isotype control antibody (eBioscience). The cells were washed, and their fluorescence intensities were measured by FACS analysis. For intracellular cytokine staining, splenocytes were stimulated with P2C-RGDS for 72 h and Brefeldin A (GolgiPlug; BD Biosciences, San Diego, CA, USA) for the last 6 h. Cells were stained with phycoerythrin-conjugated antimouse CD3e, antimouse CD4, antimouse CD8a antibodies, allophycocyanin-conjugated antimouse CD11c, or antimouse NK1.1 antibodies (eBioscience), followed by fixation and permeabilization with the Cytofix/Cytoperm plus Kit (BD Biosciences). Cells were stained intracellularly with FITC-labeled anti-IFN-γ antibody (XMG1.2; eBioscience). For ELISA, samples were stored at –80°C and analyzed with ELISA kits for IFN-γ, TNF-α, and IL12p40 (Biosource, Camarillo, CA, USA).

***In vivo* therapy model.** C57BL/6 mice were shaved on the back and injected subcutaneously with 200 μL of $1–2 \times 10^6$ syngeneic EG7 cells in PBS on Day 0. Thereafter, the treatment was performed three times, on Days 16, 20, and 23, and tumor volumes were measured using a caliper every 2–3 days. A volume of 50 μL of a mixture consisting of 10 nmol of lipopeptide and the cell lysate of 2×10^5 EG7 cells with or without 10 nmol of RGDS peptide was injected intradermally around the transplanted tumor. Tumor volume was calculated using the formula: Tumor volume (cm^3) = (long diameter) × (short diameter) × (short diameter) × 0.4. Statistical analysis was performed with the Student's *t*-test.

***Ex vivo* assay.** C57BL/6 mice were treated intradermally with a mixture of 10 nmol of lipopeptide and the cell lysate of 2×10^5 EG7 cells every 3 days for >4 treatments. At 24 h after the last treatment, the mice were sacrificed by etherization, and then the splenocytes and lymph node cells were prepared and cultured for 4 days to be primed by DCs and macrophages. The cytolytic activities of lymph node cells were then analyzed with a ^{51}Cr release assay.[18] The percentage of specific lysis was calculated using the formula: %Specific lysis = [(experimental release – spontaneous release)/(total release – spontaneous release)] × 100. The proportions of CD8- and CD11c-positive cells in the lymph nodes or spleen were analyzed by FACS.

Results

To design a new TLR2 ligand with activity equivalent to that of BCG-CWS, the minimum lipopeptide unit, P2C, was connected to the RGDS integrin-binding motif to increase adherence to DCs, forming P2C-RGDS (Fig. 1a). The hydrophobicity and pI of P2C-RGDS were similar to those of MALP-2, and the molecular weight of P2C-RGDS was half that of MALP-2 (Fig. 1b).

First, the synthetic adjuvants were tested for their capacity to activate BMDCs *in vitro* when these compounds were added to the culture medium. P2C-RGDS enhanced the expression of CD80 and CD86 in BMDCs at a level equal to that of MALP-2, the positive control (Fig. 2a). P2C-RGDS also enhanced the production of IL12p40 and TNF-α (Fig. 2b) and the proliferation of allogeneic T cells co-cultured with the BMDCs. Thus, P2C-RGDS and MALP-2 stimulate DCs equally *in vitro*, whereas P2C does not show the same activity.

Macrophage-activating lipopeptide-2 is a ligand of TLR2/6 that activates DCs through MyD88. To examine the TLR2 and TLR signaling pathway-dependence of P2C-RGDS, BMDCs were prepared from TLR2$^{-/-}$, MyD88$^{-/-}$, or TICAM-$1^{-/-}$ mice and stimulated with these synthetic lipopeptides. Both MALP-2 and P2C-RGDS enhanced the expression of CD80 and CD86 in BMDCs derived from WT or TICAM-$1^{-/-}$ mice, but not TLR2$^{-/-}$ or MyD88$^{-/-}$ mice (Fig. 3), suggesting that P2C-RGDS is a TLR2 ligand with activity similar to that of MALP-2 *in vitro*.

Next, the functional dependence of P2C-RGDS as a TLR2 ligand on not only its hydrophilicity, but also on the motif-specificity of the peptide sequences, was tested. Since MALP2 and P2C-RGDS activated DCs to the same extent at 37°C for 48 h, DCs were instead stimulated at 4°C for 1 h, then washed and re-cultured at 37°C for 48 h. Under these conditions, P2C-RGDS induced IL12p40 more efficiently than MALP-2 (Fig. 4a). To analyze the specificity of the RGDS peptide,

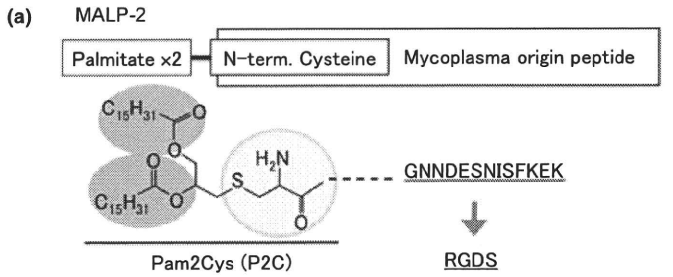

(b)

Compounds		M.W.	Peptide	pI	Hydrophobicity
P2C		672.5	P2 C	—	—
MALP-2	(N)	2134.1	P2 C G N N D E S N I S F K E K	*4.68	−1.5
FSL-1	(N)	1666.1	P2 C G D P K H P K S F	8.21	−1.36
P2C-SKKKK	(S)	1271.8	P2 C S K K K K	10.04	−2.32
P2C-RGDS	(S)	1087.5	P2 C R G D S	*5.83	−1.34

Fig. 1. The structure of the adjuvant developed in the present study, a synthetic Toll-like receptor (TLR)-2 ligand containing the RGDS motif. (a) The structure of macrophage-activating lipopeptide (MALP)-2. The N-terminal cysteine of a peptide derived from a mycobacterium is modified with 2 palmitates [Pam2Cys, P2C, S-(2,3-bispalmitoyloxypropyl)cysteine]. RGDS was conjugated to P2C to form P2C-RGDS because of its hydrophilicity and its additional function as an integrin-binding motif for cell adhesion. (b) The structure, molecular weight, isoelectric point (pI), and hydrophobicity of synthetic (P2C-RGDS, P2C-SKKKK) and natural (MALP-2, FSL-1) lipopeptides used in this study. The pI and hydrophobicity of the peptide were calculated using ProtParam tools (http://br.expasy.org/tools/protparam.html). The pI and hydrophobicity of P2C-RGDS were almost equivalent to those of MALP-2. The molecular weight of P2C-RGDS was about half that of MALP-2. N, natural TLR2 ligand; S, synthetic TLR2 ligand. The asterisks (*) indicate acidic peptides. The gray boxes indicate hydrophobic amino acids.

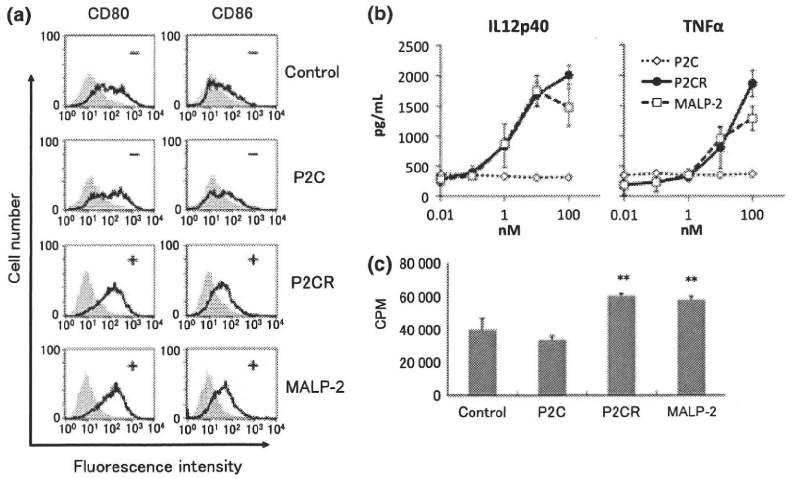

Fig. 2. P2C-RGDS activates bone marrow-derived dendritic cells (BMDCs) as much as macrophage-activating lipopeptide (MALP)-2 *in vitro*. (a) The enhancement of CD80/CD86 expression of BMDCs stimulated with the indicated compounds (100 nM) for 24 h was observed by FACS analysis. (b) Interleukin (IL)12p40 and tumor necrosis factor (TNF)-α production in BMDCs stimulated with each compound for 48 h was determined by ELISA. (c) The proliferation of allogeneic T cells co-cultured with activated-BMDCs for 72 h was measured by the [^{3}H] thymidine uptake method. Bone marrow-derived dendritic cells were treated with each compound for 24 h before co-culture with T cells. CPM, count per minute. $^{**}P < 0.01$ *vs* control (Student's *t*-test). P2CR, P2C-RGDS.

IL12p40 production was inhibited by the addition of an RGDS competitor peptide or anti-integrin β1 antibody to the assay. The addition of the RGDS competitor peptide and the integrin blocking antibodies partially attenuated the production of IL12p40 induced by P2C-RGDS, but not that induced by MALP-2 (Fig. 4b,c). These results indicate that not only hydrophilicity but also the functional RGDS motif contributes to the activation of DCs *in vitro* at short incubation times.

The P2C-RGDS-induced production of IFN-γ was evaluated next, using *in vitro* whole splenocyte stimulation. The activities of P2C-RGDS and MALP-2, as measured by IFN-γ production, were comparable and weaker than that of BCG-CWS when splenocytes were simply stimulated with each compound for 72 h (Fig. 5a). However, when splenocytes were stimulated with each compound at 4°C for 1 h and re-cultured at 37°C for 72 h, the P2C-RGDS-induced production of IFN-γ was stronger than that induced by MALP-2 and it was attenuated mostly by the RGDS peptide. Furthermore, the splenocytes stimulated with P2C-RGDS produced as much IFN-γ as those stimulated with BCG-CWS at 4°C for 1 h (Fig. 5b). Interferon-γ production was not detected in splenocytes depleted of CD11c-positive dendritic cells, and IFN-γ production could be restored under these conditions by adding back CD11c-positive cells. These data indicate that IFN-γ production by splenocytes following stimulation with

doi: 10.1111/j.1349-7006.2010.01583.x

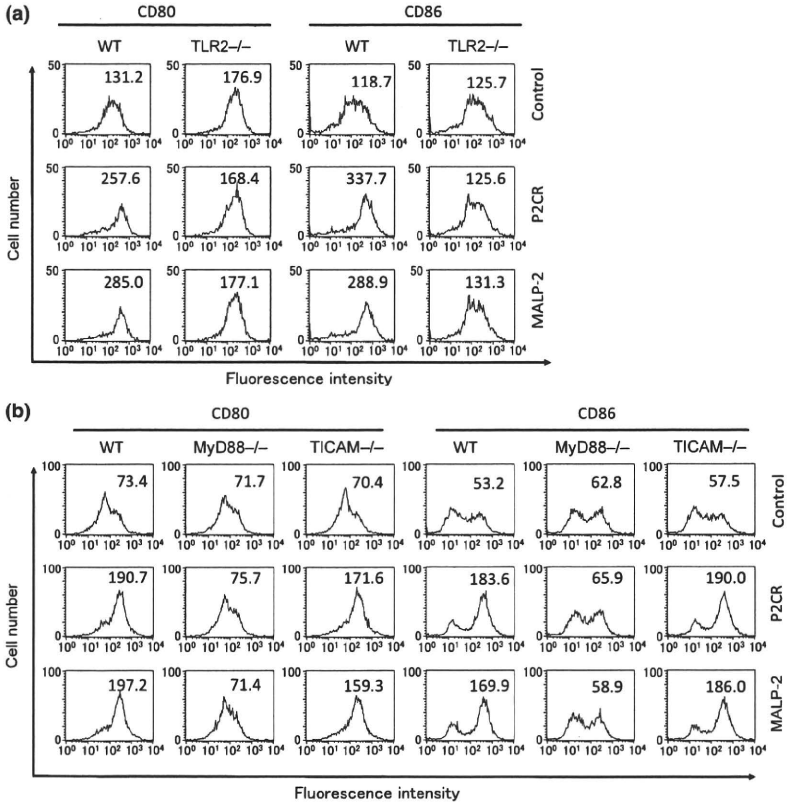

Fig. 3. P2C-RGDS activates bone marrow-derived dendritic cells (BMDCs) in a Toll-like receptor (TLR)-2 and myeloid differentiation protein (MyD)-88-dependent manner *in vitro*. (a,b) Bone marrow-derived dendritic cells were prepared from mice lacking TLR2 ($TLR2^{-/-}$) and TLR adaptor molecules ($MyD88^{-/-}$ and $TICAM\text{-}1^{-/-}$). CD80 and CD86 expression was observed by FACS analysis at 24 h after BMDCs were stimulated with MALP-2 or P2C-RGDS. The numbers in the panels represent mean fluorescence intensities. P2C-RGDS and MALP-2 activated BMDCs via TLR2 and MyD88, but not via the Toll/IL-1 receptor homology-containing adaptor molecule (TICAM)-1 pathway. P2CR, P2C-RGDS.

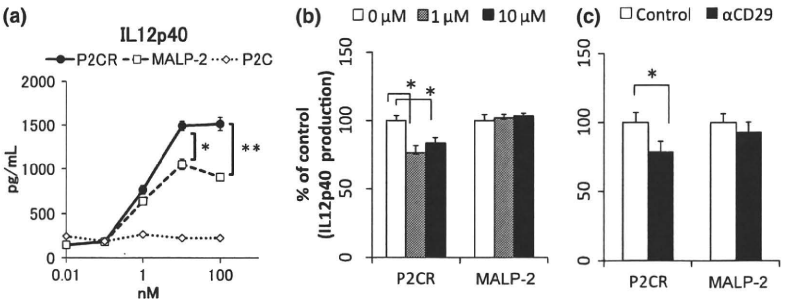

Fig. 4. P2C-RGDS efficiently activates bone marrow-derived dendritic cells (BMDCs) in an RGDS motif–dependent manner *in vitro* over short incubation times. (a) Interleukin (IL)12p40 production of BMDCs stimulated with each Toll-like receptor (TLR)-2 ligand at 4°C for 1 h. Bone marrow-derived dendritic cells were washed after the stimulation and re-cultured for 48 h. Interleukin12p40 production was determined by ELISA. (b) Bone marrow-derived dendritic cells were pretreated with the indicated concentrations of RGDS peptide (P2C-modification free) as a competitor at 4°C for 30 min. Then, the BMDCs were stimulated with TLR2 ligands (10 nM) at 4°C for 1 h. Interleukin12p40 production by BMDCs was determined by ELISA. Data are shown as percentages of each control value. (c) The inhibition effects of α-CD29 (integrin β1) antibody on IL12p40 production of BMDCs. Bone marrow-derived dendritic cells were pre-treated with 10 μg/mL of each antibody at 4°C for 30 min before stimulation. P2CR, P2C-RGDS.

P2C-RGDS was mediated by DC activation (Fig. 5c). IFN-γ production was also impaired by depletion of CD90 (Thy1)-positive T cells (Fig. 5c). Further assessment of IFN-γ producing cells by intracellular cytokine staining revealed that IFN-γ was mainly detected in CD3- or CD8-positive cells, and in CD4-, NK1.1-, or CD11c-negative cells stimulated with P2C-RGDS (Fig. 5d).

Finally, the antitumor activity of P2C-RGDS *in vivo* was investigated using a tumor-implantation model. The mice were transplanted with EG7 on day 0, and treated with synthetic lipopeptide (10 nmol) and the cell lysate of EG7 cells (2×10^5) on Days 16, 20, and 23. The minimum lipopeptide unit P2C showed no *in vivo* antitumor activity similar to the activation of DCs *in vitro*. Although MALP-2-treated mice showed a slightly smaller tumor volume than control mice, this difference was not significant. However, P2C-RGDS showed a significant antitumor effect (Student's *t*-test, $P < 0.05$ *vs* control; Fig. 6a). Moreover, the mixture of P2C and the RGDS peptide showed no antitumor activity (Fig. 6b). Next, lymph node cells from mice immunized with EG7 lysate and P2C-RGDS or MALP-2 were isolated, and the cytotoxicity against EG7 and B16D8 cells was measured using a ^{51}Cr release assay. P2C-RGDS specifically

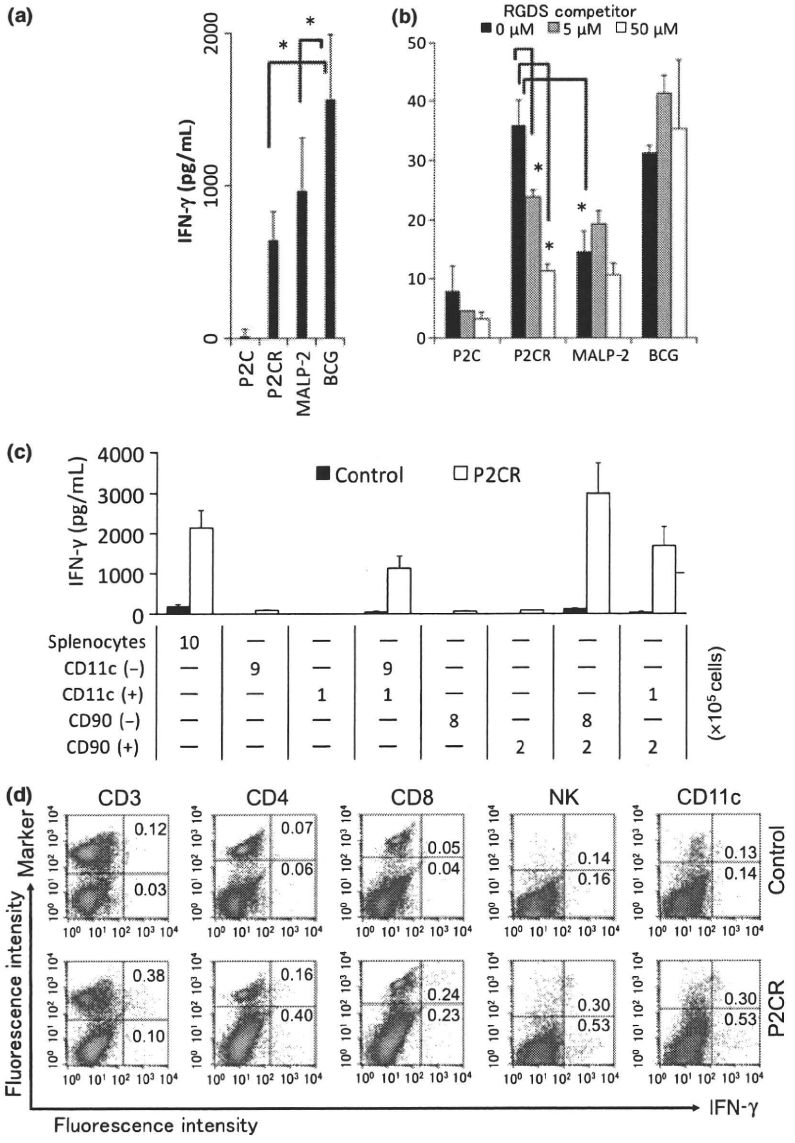

Fig. 5. P2C-RGDS efficiently activates splenocytes in an RGDS motif-dependent manner. (a) Interferon (IFN)-γ production by splenocytes stimulated with each compound for 72 h. (b) The effect of RGDS competitor peptide pretreatment on IFN-γ production. The RGDS competitor attenuated IFN-γ production from splenocytes stimulated with P2C-RGDS at 4°C for 1 h. (c) The roles of CD11c-positive cells (dendritic cells) and CD90-positive cells (T cells) on IFN-γ production by splenocytes. The splenocytes were separated into $CD11c^+$ and $CD11c^-$ cells, or $CD90^+$ and $CD90^-$ cells by using MACS beads. Cells were prepared based on the recovery ratio and stimulated with P2C-RGDS for 72 h. $*P < 0.05$, $**P < 0.01$ (Student's *t*-test); n.d, not detected. (d) Intracellular IFN-γ staining of splenocytes with various expression markers. Density plots show the expression of each surface marker and intracellular staining for IFN-γ, and the numbers indicate the proportion of IFN-γ-positive cells (%). P2CR, P2C-RGDS.

induced a stronger cytotoxic activity against EG7 than MALP-2, but the lymph node cells were not sufficiently cytotoxic against the negative target B16D8 cells (Fig. 6c). In addition, lymph node cells were cultured continuously with live EG7 cells for 96 h and the proportion of CD8-positive cells was analyzed by FACS. CD8-positive cells in lymph nodes derived from P2C-RGDS-treated mice remained at a level of approximately 16% of total cells, but most CD8-positive cells from MALP-2-treated mice were lost after culture with EG7 (Fig. 6d). The proportion of CD8-positive cells in a splenocyte population derived from immunized mice was also evaluated using FACS analysis. CD8-positive cells were proportionally higher among splenocytes derived from mice treated with P2C-RGDS than among splenocytes derived from mice treated with MALP-2 (Fig. 6e). Necrosis was observed on the surface of tumors after P2C-RGDS but not after MALP-2 treatment, and CD8-positive cells were detected around the necrosis tissue by immunostaining (data not shown). These data suggest that P2C-RGDS induces and activates CTLs more efficiently than MALP-2. Moreover, to analyze the mechanism underlying the strong antitumor effect of P2C-RGDS *in vivo*, the proportions of CD11c-positive cells in draining lymph nodes were analyzed in mice treated with MALP-2 or P2C-RGDS for 24 h. P2C-RGDS induced the migration of CD11c-positive cells to the draining lymph nodes more effectively than MALP2 ($P = 0.055$, Fig. 6f).

Discussion

Natural TLR2 ligands of bacterial origin, such as MALP-2[31,41,42] and FSL-1,[32] have been reported to effectively activate CD8-positive T cells and induce antitumor activity. Because these lipopeptides are hydrophilic, it was predicted that the hydrophilicity of the peptide might be important for its activity.[31–34] Several researchers have relied on a chemobiologic strategy of producing amino acid replacements to explore which portion of the lipopeptide sequence possesses effective adjuvant activity.[43] Using this strategy, Takeda developed Tan-1511 analogues that show high levels of activity in the induction of granulopoiesis.[43] Another strategy has been to randomly search for sequences or peptides effective at enhancing TLR2 ligand

doi: 10.1111/j.1349-7006.2010.01583.x

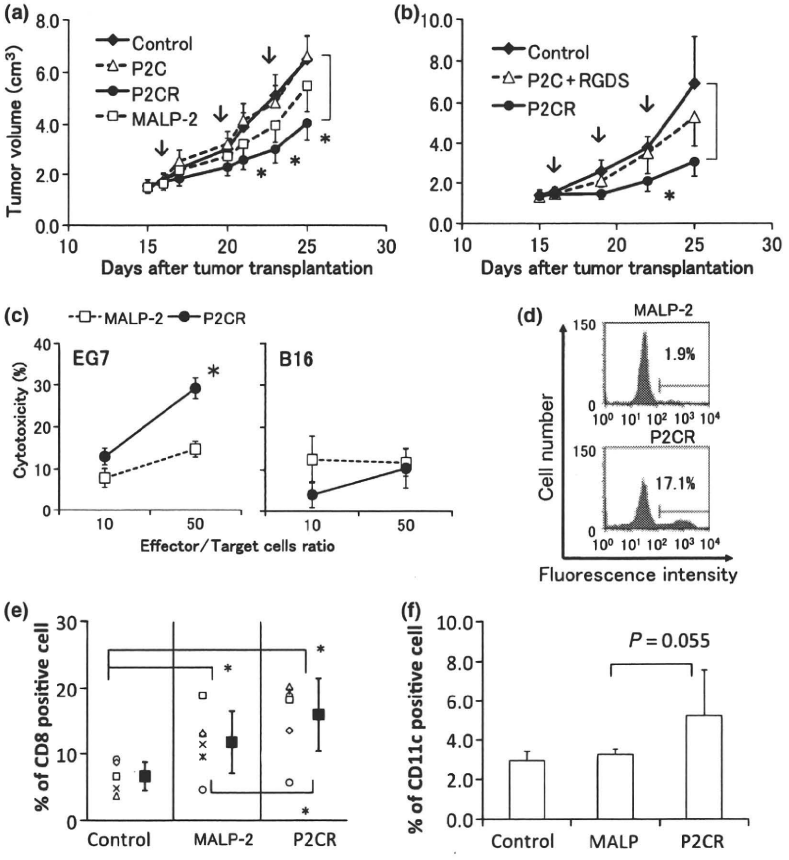

Fig. 6. P2C-RGDS is more effective at retarding tumor growth and inducing CD8-positive cells than macrophage-activating lipopeptide (MALP)-2 *in vivo* and *ex vivo*. Antitumor effect of P2C-RGDS and MALP-2 (a), and of a mixture of P2C and RGDS peptide (b), in the EG7-implanted mouse model (C57BL6-EG7 model). Mice were treated with Toll-like receptor (TLR)-2 ligand and EG7 lysate on Days 16, 20, and 23 (arrows). The data are shown as means ± SE ($n = 9$). *$P < 0.05$ *vs* control (Student's *t*-test). (c) Lymph node cells derived from P2C-RGDS and EG7 lysate-immunized mice showed stronger cytotoxicity than cells from MALP-2-immunized mice against EG7 but not B16 (^{51}Cr release assay). *$P < 0.05$ *vs* MALP-2 (Student's *t*-test). (d) CD8-positive T cells were more effectively induced in lymph nodes derived from mice immunized with P2C-RGDS and EG7 lysate than in those immunized with MALP-2. The lymph node cells in Figure 6(c) were cultured with live EG7 for 96 h, and then the proportion of CD8-positive T cells was analyzed. (e) Immunization with P2C-RGDS and EG7 lysate induced CD8-positive T cells in splenocytes more efficiently than immunization with MALP-2. The proportions of CD8-positive cells in splenocytes were determined by FACS analysis at 96 h after the initiation of splenocyte cultivation. Each symbol indicates an individual experiment. The closed squares represent average ± SD. *$P < 0.05$ (paired *t*-test). (f) The proportion of CD11c-positive cells in the draining lymph nodes at 24 h after immunization. CD11c-positive cells were examined by FACS analysis. $P = 0.055$ *vs* MALP-2 (Student's *t*-test). P2CR, P2C-RGDS.

activity.[44] The purpose of the current project was to design a TLR2 ligand with an additional function through the addition of a hydrophilic, functional peptide that could be developed as a new synthetic adjuvant (Fig. 1). In comparison to a prior developmental strategies, the present design has the advantage of allowing the selection of various functions, and because the designed lipopeptides do not exist in nature, they could show new or enhanced properties. In the present study, the TLR2 ligand was designed to possess stronger adhesive capacity through the linking of the RGDS peptide to P2C.

The compound P2C-RGDS was developed and shown to be as effective as MALP-2 in generating BMDC responses *in vitro*, such as the enhancement of a maturation marker (CD80 and CD86) and cytokine induction when DCs were cultured with each compound for 24–48 h (Fig. 2). P2C-RGDS and MALP-2 also activated DCs through the TLR2–MyD88 pathway (Fig. 3),[38] but P2C-RGDS activated DCs more efficiently than MALP2, and the RGDS integrin binding motif was found to be important for DCs activation over short incubation times (Fig. 4). Because DCs were treated with compounds for only 1 h, then washed and re-cultured at 37°C for 48 h in these experiments, it was predicted that P2C-RGDS might efficiently adhere to the DCs in short incubation times, and then stimulate DCs continuously at the surface or in the phagosome of DCs. Whole splenocytes stimulated with P2C-RGDS also produced more IFN-γ than MALP-2 over short incubation times (Fig. 5b), and the production of IFN-γ by splenocytes depended on CD11c-positive DCs (Fig. 5c). These data suggest that the adhesion properties of P2C-RGDS caused the efficient activation of DCs, and reflected splenocyte activation. The stronger IFN-γ induction by P2C-RGDS might also be due to its retention in the culture system by adherence to various cells among the splenocytes. Moreover, P2C-RGDS may be retained in local regions for a long time via integrin binding *in vivo*, leading to the efficient activation of immune cells such as dermal DCs. P2C-RGDS induced the migration of CD11c-positive cells into the draining lymph nodes more effectively than MALP-2 in *in vivo* experiments (Fig. 6f). These DCs might activate CD8-positive cells, enhance cytotoxicity (Fig. 6c), and lead to retardation of tumor growth (Fig. 6a). These data suggest that the greater activation of DCs by P2C-RGDS compared to MALP2 influences IFN-γ production by splenocytes, thereby resulting in increased cytotoxicity and antitumor effects *in vivo*.

The induction of IFN-γ production by BCG-CWS treatment is one of the indexes for continuing treatment in clinical applications,[14,19] and the response can be confirmed in mouse experiments. Interferon-γ stimulation up-regulates the expression of MHC class I in tumor cells,[45] presumably improving tumor recognition by immune cells, and leading to increased suppression of tumor growth. With short stimulation periods, P2C-RGDS induced as much IFN-γ as BCG-CWS. Although the present compound was designed without considering IFN-γ induction, results show that CD8-positive cells produced IFN-γ in splenocytes stimulated with P2C-RGDS alone in the absence of antigen peptide (Fig. 5). The mechanism of IFN-γ induction by P2C-RGDS should be analyzed in the future. The tumor volume of the BCG-CWS treatment group was about 60% of that of the control on Day 22 (data not shown), and the therapeutic effects of P2C-RGDS were almost equivalent to those of BCG-CWS. Because BCG-CWS must be emulsified with drakeol, the use of P2C-RGDS has significant advantages.

The integrin binding sequence has served as the basis for the design of drugs that depend on adhesive activity. In the present work, this adhesive function was applied to TLR ligands to enhance immunoadjuvant activity. Cilengitide, a cyclic RGD peptide, was developed as an integrin αV antagonist, which impairs angiogenesis, tumor growth, and metastasis[46] because integrins are expressed on various tumor cells.[47] Although EG7 expresses integrin αV, β1, and β3, P2C-RGDS and RGDS peptide did not show direct cytotoxic activity against EG7 cells at concentrations up to 100 nM (data not shown). Furthermore, the adjuvant activities of P2C-RGDS were compared to those of a mixture of P2C and RGDS peptide. P2C had no adjuvant activity, such as the activation of DCs and splenocytes *in vitro* or antitumor effect *in vivo* by lipopeptides (Figs 2b, 5a, 6a). The mixture did not show any effects *in vivo* such as appreciable antitumor activity (Fig. 6b). Based on these results, the stronger antitumor activity of P2C-RGDS compared to that of MALP-2 is thought to occur through an increase in cell adhesive ability, but not through the inhibition of angiogenesis.

Concerning the relationship between TLR and its ligand, it is suggested that a co-receptor plays a key role for TLR binding and signaling[1,7,48] as observed previously for CD14 in the Lipopolysaccharide (LPS)–TLR4 signaling pathway. Although integrin binding is predicted to support the capture and phagocytosis of ligands by DCs, integrin signaling in addition to TLR signaling might influence adjuvant activity. Stronger adjuvants will be developed by selecting for other properties, in addition to TLR signaling, that are essential for adjuvant activity, and the integrin signal could be one of the candidates.

In the present work, the inclusion of an integrin-binding motif in a TLR2 ligand was examined for its effect in increasing the activity of the compound as an antitumor adjuvant by enhancing adhesion of the ligand to DCs and other cells. Dendritic cells efficiently recognized P2C-RGDS, which they adhered to and maintained around cells, and P2C-RGDS showed stronger antitumor activity than MALP-2 *in vivo*. The present adjuvant-engineering project is a new strategy to incorporate biological findings into drug design. Targeting peptides are used to elicit a strictly selective response among immune cells. A targeted strategy can effectively activate immune cells at a low concentration while not affecting other cells whose activation might lead to side effects. More than 20 TLR2 ligands with 10 alternative functions have already been synthesized by adjuvant engineering and our group is working to develop the strongest adjuvant through continued evaluation and improvements.

Acknowledgments

This work was supported in part by KAKENHI (15790069; 19790301; 20200075; 21790400) from the Ministry of Education, Culture, Science, and Technology of Japan; The Uehara Memorial Foundation; Osaka Community Foundation; and The Charitable Trust Osaka Cancer Researcher Fund. We are grateful to Drs K. Toyoshima, H. Koyama, S. Imaoka, S. Hori, K. Kato, and M. Tatsuta (Osaka Medical Center for Cancer, Osaka) for their support of this work. We are grateful to Dr K. Kikuchi (Sapporo Medical University, Sapporo), who gave the name ''adjuvant engineering'' to our project. Thanks are also due to N. Kanto, and T. Yasuda, E. Takahara, Y. Mimura, and M. Yabu (Osaka Medical Center for Cancer, Osaka) for their assistance.

References

1 Seya T, Akazawa T, Tsujita T, Matsumoto M. Role of Toll-like receptors in adjuvant-augmented immune therapies. *Evid Based Complement Alternat Med* 2006; **3**(1): 31–8.
2 Akazawa T, Ebihara T, Okuno M *et al.* Antitumor NK activation induced by the Toll-like receptor 3-TICAM-1 (TRIF) pathway in myeloid dendritic cells. *Proc Natl Acad Sci U S A* 2007; **104**(1): 252–7.
3 Okamoto M, Oshikawa T, Tano T *et al.* Involvement of Toll-like receptor 4 signaling in interferon-g production and antitumor effect by streptococcal agent OK-432. *J Natl Cancer Inst* 2003; **95**(4): 316–26.
4 Rosenberg SA, Yang JC, Restifo NP. Cancer immunotherapy: moving beyond current vaccines. *Nat Med* 2004; **10**(9): 909–15.
5 Celis E. Toll-like receptor ligands energize peptide vaccines through multiple paths. *Cancer Res* 2007; **67**(17): 7945–7.
6 Kanzler H, Barrat FJ, Hessel EM, Coffman RL. Therapeutic targeting of innate immunity with Toll-like receptor agonists and antagonists. *Nat Med* 2007; **13**(5): 552–9.
7 Seya T, Akazawa T, Uehori J, Matsumoto M, Azuma I, Toyoshima K. Role of toll-like receptors and their adaptors in adjuvant immunotherapy for cancer. *Anticancer Res* 2003; **23**(6a): 4369–76.
8 Akira S, Uematsu S, Takeuchi O. Pathogen recognition and innate immunity. *Cell* 2006; **124**: 783–801.
9 Miconnet I, Coste I, Beermann F *et al.* Cancer vaccine design: a novel bacterial adjuvant for peptide-specific CTL induction. *J Immunol* 2001; **166**(7): 4612–19.
10 Iwasaki A, Medzhitov R. Toll-like receptor control of the adaptive immune responses. *Nat Immunol* 2004; **5**: 987–95.
11 Kaisho T, Akira S. Toll-like receptors as adjuvant receptors. *Biochim Biophys Acta* 2002; **1589**(1): 1–13.
12 Hemmi H, Takeuchi O, Kawai T *et al.* A Toll-like receptor recognizes bacterial DNA. *Nature* 2000; **408**(6813): 740–5.
13 Azuma I, Ribi EE, Meyer TJ, Zbar B. Biologically active components from mycobacterial cell walls: I Isolation and composition of cell wall skeleton and component P3. *J Natl Cancer Inst* 1974; **52**: 95–101.
14 Hayashi A, Doi O, Azuma I, Toyoshima K. Immuno-friendly use of BCG-cell wall skeleton remarkably improves the survival rate of various cancer patients. *Proc Jpn Acad* 1998; **74** Ser. B: 50–5.
15 Uehori J, Fukase K, Akazawa T *et al.* Dendritic cell maturation induced by muramyl dipeptide (MDP) derivatives: monoacylated MDP confers TLR2/TLR4 activation. *J Immunol* 2005; **174**(11): 7096–103.
16 Tsuji S, Matsumoto M, Takeuchi O *et al.* Maturation of human dendritic cells by cell wall skeleton of Mycobacterium bovis bacillus Calmette-Guérin: involvement of toll-like receptors. *Infect Immun* 2000; **68**: 6883–90.
17 Uehori J, Matsumoto M, Tsuji S *et al.* Simultaneous blocking of human Toll-like receptor 2 and 4 suppresses myeloid dendritic cell activation induced by Mycobacterium bovis bacillus Calmette-Guérin (BCG)-peptidoglycan (PGN). *Infect Immun* 2003; **71**: 4238–49.
18 Akazawa T, Masuda H, Saeki Y *et al.* Adjuvant-mediated tumor regression and tumor-specific cytotoxic response are impaired in MyD88-deficient mice. *Cancer Res* 2004; **64**(2): 757–64.
19 Kodama K, Higashiyama M, Takami K *et al.* Innate immune therapy with a Bacillus Calmette-Guérin cell wall skeleton after radical surgery for non-small cell lung cancer: a case-control study. *Surg Today* 2009; **39**(3): 194–200.
20 Begum NA, Ishii K, Kurita-Taniguchi M *et al.* Mycobacterium bovis BCG cell wall-specific differentially expressed genes identified by differential display and cDNA subtraction in human macrophages. *Infect Immun* 2004; **72**(2): 937–48.
21 Matsumoto M, Seya T, Kikkawa S *et al.* Interferon gamma-producing ability in blood lymphocytes of patients with lung cancer through activation of the innate immune system by BCG cell wall skeleton. *Int Immunopharmacol* 2001; **1**(8): 1559–69.
22 Oppmann B, Lesley R, Blom B *et al.* Novel p19 protein engages IL-12p40 to form a cytokine, IL-23, with biological activities similar as well as distinct from IL-12. *Immunity* 2000; **13**(5): 715–25.
23 Zou JP, Yamamoto N, Fujii T *et al.* Systemic administration of rIL-12 induces complete tumor regression and protective immunity: response is correlated with a striking reversal of suppressed IFN-g production by anti-tumor T cells. *Int Immunol* 1995; **7**(7): 1135–45.
24 Langowski JL, Zhang X, Wu L *et al.* IL-23 promotes tumour incidence and growth. *Nature* 2006; **442**(7101): 461–5.
25 Kolls JK, Lindén A. Interleukin-17 family members and inflammation. *Immunity* 2004; **21**(4): 467–76.
26 Shime H, Yabu M, Akazawa T *et al.* Tumor-secreted lactic acid promotes IL-23/IL-17 proinflammatory pathway. *J Immunol* 2008; **180**(11): 7175–83.
27 Kaiga T, Sato M, Kaneda H, Iwakura Y, Takayama T, Tahara H. Systemic administration of IL-23 induces potent antitumor immunity primarily mediated through Th1-type response in association with the endogenously expressed IL-12. *J Immunol* 2007; **178**(12): 7571–80.
28 Jackson DC, Lau YF, Le T *et al.* A totally synthetic vaccine of generic structure that targets Toll-like receptor 2 on dendritic cells and promotes

doi: 10.1111/j.1349-7006.2010.01583.x